Biogeosciences

Dynamics of air–sea CO$_2$ fluxes in the northwestern European shelf based on voluntary observing ship and satellite observations

P. Marrec[1,2], **T. Cariou**[1,2], **E. Macé**[1,2], **P. Morin**[1,2], **L. A. Salt**[1,2], **M. Vernet**[1,2], **B. Taylor**[3], **K. Paxman**[3], and **Y. Bozec**[1,2]

[1]CNRS, UMR7144, Equipe Chimie Marine, Station Biologique de Roscoff, Place Georges Teissier, 29680 Roscoff, France
[2]Sorbonne Universités, UPMC, Univ. Paris 06, UMR7144, Adaptation et Diversité en Milieu Marin, Station Biologique de Roscoff, 29680 Roscoff, France
[3]Remote Sensing Group, Plymouth Marine Laboratory, Prospect Place PL1 3DH, UK

Correspondence to: P. Marrec (pmarrec@sb-roscoff.fr)

Abstract. From January 2011 to December 2013, we constructed a comprehensive pCO$_2$ data set based on voluntary observing ship (VOS) measurements in the western English Channel (WEC). We subsequently estimated surface pCO$_2$ and air–sea CO$_2$ fluxes in northwestern European continental shelf waters using multiple linear regressions (MLRs) from remotely sensed sea surface temperature (SST), chlorophyll a concentration (Chl a), wind speed (WND), photosynthetically active radiation (PAR) and modeled mixed layer depth (MLD). We developed specific MLRs for the seasonally stratified northern WEC (nWEC) and the permanently well-mixed southern WEC (sWEC) and calculated surface pCO$_2$ with uncertainties of 17 and 16 µatm, respectively. We extrapolated the relationships obtained for the WEC based on the 2011–2013 data set (1) temporally over a decade and (2) spatially in the adjacent Celtic and Irish seas (CS and IS), two regions which exhibit hydrographical and biogeochemical characteristics similar to those of WEC waters. We validated these extrapolations with pCO$_2$ data from the SOCAT and LDEO databases and obtained good agreement between modeled and observed data. On an annual scale, seasonally stratified systems acted as a sink of CO$_2$ from the atmosphere of -0.6 ± 0.3, -0.9 ± 0.3 and -0.5 ± 0.3 mol C m^{-2} yr^{-1} in the northern Celtic Sea, southern Celtic sea and nWEC, respectively, whereas permanently well-mixed systems acted as source of CO$_2$ to the atmosphere of 0.2 ± 0.2 and 0.3 ± 0.2 mol C m^{-2} yr^{-1} in the sWEC and IS, respectively. Air–sea CO$_2$ fluxes showed important inter-annual variability resulting in significant differences in the intensity and/or direction of annual fluxes. We

scaled the mean annual fluxes over these provinces for the last decade and obtained the first annual average uptake of -1.11 ± 0.32 Tg C yr^{-1} for this part of the northwestern European continental shelf. Our study showed that combining VOS data with satellite observations can be a powerful tool to estimate and extrapolate air–sea CO$_2$ fluxes in sparsely sampled area.

1 Introduction

Continental shelf seas form a complex interplay between the land, ocean and atmosphere, hosting a multitude of biogeochemical processes (Walsh, 1991; Liu et al., 2010) and play a key role in the global carbon cycle (Walsh et al., 1981; Muller-Karger et al., 2005; Bauer et al., 2013). Even though marginal seas occupy only 7 % of global oceanic area, they host enhanced biological activity, which accounts for 15 to 30 % of global oceanic primary production (Gattuso et al., 1998). These productive regions are characterized by enhanced air–sea CO$_2$ fluxes compared to open oceans (Tsunogai et al., 1999; Thomas et al., 2004) and are particularly vulnerable to anthropogenic forcings such as eutrophication and ocean acidification (Borges and Gypens, 2010; Borges et al., 2010a; Wallace et al., 2014). In a context of climate change, with rising anthropogenic CO$_2$ levels in the atmosphere and the oceans (IPCC, 2013), it is essential to better constrain carbon cycle dynamics and particularly air–sea CO$_2$ fluxes. Given the large diversity and heterogeneity of coastal ecosystems, this goal remains challenging. Rapid ex-

pansion of partial pressure of CO_2 (pCO_2) observations over the past decade have allowed the first assessments of the contribution of coastal ecosystems in terms of global air–sea CO_2 fluxes (Borges et al., 2005; Cai et al., 2006; Chen and Borges, 2009; Cai, 2011). However, extrapolation from local to global estimates still involves large uncertainties and many continental shelf seas remain under-sampled.

Accurate estimates of air–sea CO_2 fluxes in continental shelf seas still suffer from lack of sufficient spatial and temporal coverage. Surveys based on seasonal sampling during oceanographic campaigns and time series at fixed locations are limited due to the large temporal and spatial variability of these systems. The use of voluntary observing ships (VOSs) can improve the coverage of coastal areas at a lesser cost. The recent advances made in this field (Schneider et al., 2006, 2014; Padin et al., 2007; Omar et al., 2010; Marrec et al., 2014) can be combined with other new approaches. Since the 2000s, pCO_2 predictions based on remote sensing techniques have been successfully developed for open ocean areas (Lefèvre et al., 2002; Ono et al., 2004; Olsen et al., 2004; Rangama et al. 2005; Gledhill et al., 2008; Padin et al., 2009; Chierici et al., 2009, 2012). These estimates were based on the use of multiple linear regressions (MLRs) to relate surface ocean pCO_2 to sea surface temperature (SST), chlorophyll a concentration (Chl a) and occasionally also mixed layer depth (MLD), sea surface salinity (SSS) or geographical position (latitude and longitude). More complex neural networks techniques using self-organizing maps have also given promising results (Lefèvre et al., 2005; Telszewski et al. 2009; Friedrich and Oschlies, 2009). In continental shelf seas the development of remotely sensed approaches is more challenging because of higher temporal and spatial variability of biogeochemical processes. The complex optical properties of these systems can also impede computations based on satellite ocean-color data. These techniques have nevertheless been used to conduct successful assessments of pCO_2 variability in coastal areas (Lohrenz and Cai, 2006; Salisbury et al., 2008; Borges et al., 2010b; Shadwick et al., 2010; Hales et al., 2012; Jo et al., 2012; Signorini et al., 2013).

To efficiently constrain surface pCO_2 in dynamic shelf seas from remotely sensed data, a comprehensive pCO_2 data set with sufficient spatial and temporal resolution is essential. In addition to a robust intra-annual temporal resolution, acquisition of pCO_2 measurements over several years is necessary in order to take into consideration the important inter-annual variability of biogeochemical processes in coastal seas. From 2011 to 2013, we collected an extensive pCO_2 data set based on VOS observations in the western English Channel (WEC), which is part of the northwestern European continental shelf (NWES). Marrec et al. (2013, 2014) assessed for the first time the seasonal and latitudinal dynamics of pCO_2 and air–sea CO_2 fluxes in the WEC, whereas previous studies of the CO_2 system in the WEC were either based on longitudinal transects (Borges and Frankignoulle, 2003; Padin et al., 2007; Dumousseaud et al., 2010) or a fixed

station approach (Kitidis et al., 2012). Air–sea CO_2 flux and pCO_2 dynamics in the North Sea have been well constrained (Thomas et al., 2004, 2005; Bozec et al., 2006; Schiettecatte et al., 2007; Prowe et al., 2009; Omar et al., 2010), but ocean carbon variability in other part of the NWES as the Celtic Sea (CS) and the Irish Sea (IS) is still poorly documented (Frankignoulle and Borges, 2001).

In this study, we will focus on the WEC, CS and IS provinces of the NWES in order to describe the dynamics of pCO_2 and air–sea CO_2 fluxes in these areas over a decade. We used MLR in WEC to develop algorithms to predict surface pCO_2 and air–sea CO_2 fluxes from remotely sensed SST, chlorophyll a concentrations (Chl a), wind speeds (WNDs), photosynthetically active radiation (PAR) and from modeled mixed layer depth (MLD). We extrapolated the relationships obtained in the WEC based on the 2011–2013 data set (1) temporally over a decade and (2) spatially in the adjacent CS and IS, two regions where pCO_2 data are very sparse. Based on the reconstructed decadal data set, we investigated the variability of pCO_2 and air–sea CO_2 fluxes over the shelf.

2 Study area

The WEC forms part of the northwestern European continental shelf, one of the world's largest margins. We studied this area from January 2011 with a VOS (Fig. 1) equipped with an autonomous ocean observing system, called Ferry-Box, featuring several sensors (Sect. 3.1, Marrec et al., 2013, 2014). This area is characterized by relatively shallow depths and intense tidal streams with maximum speeds ranging from 0.5 to $2.5 \, \text{m s}^{-1}$ (Pingree, 1980; Reid et al., 1993). Along the French coast (southern WEC – sWEC), where the tidal currents are the strongest, the water column remains vertically mixed (Wafar et al., 1983; L'Helguen et al., 1996), whereas near the English coast (northern WEC – nWEC), where tidal streams are less intense, seasonal stratification occurs (Smyth et al., 2009). Between these two distinct structures, a frontal zone oscillates, separating well-mixed and stratified waters (Pingree et al., 1975). In this complex hydrographical context, high-frequency measurements from Ferry-Box data allowed us to precisely locate this thermal front and to accurately identify the real extent of each hydrographical province (Marrec et al, 2014).

Satellite SST data (Fig. 2, Sect. 3.2) combined with Ferry-Box measurements allowed us to further define the different hydrographical provinces of the northwestern European continental shelf. Water column characteristics similar to those in the WEC are also observed in adjacent seas, i.e., the Irish Sea (IS) and the Celtic Sea (CS; Pingree and Griffiths, 1978; Pingree, 1980; Holligan, 1981; Simpson et al., 1981; Hill et al., 2008). Figure 2 shows averaged July and August SST from 2003 to 2013 between 48 and 53° N and 3.5 and 10° W. The coolest surface waters indicate areas where the water
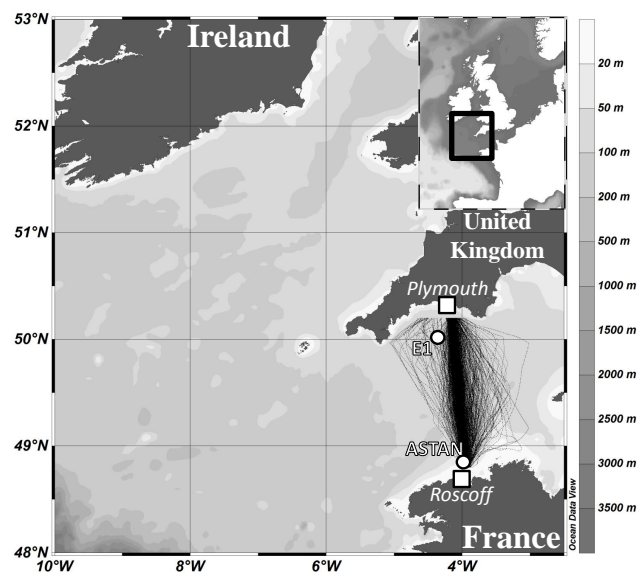
Figure 1. Map and bathymetry of the study area with the tracks of all crossings made from 2011 to 2013 by the ferry *Armorique* between Roscoff (France) and Plymouth (UK). The locations of fixed stations E1 (Western Channel Observatory) and ASTAN (coastal observatory SOMLIT) are also indicated.
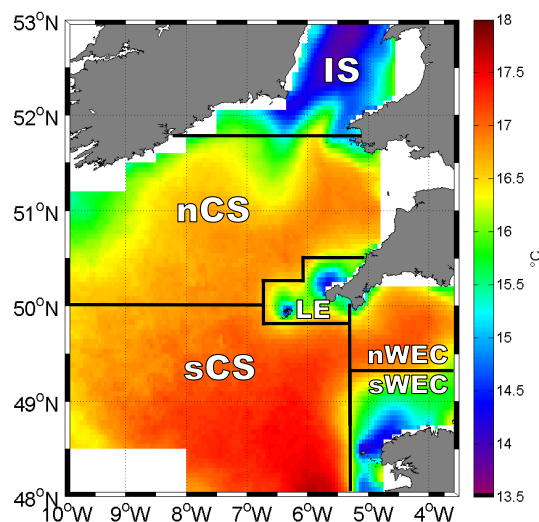

Figure 2. Mean July and August satellite SST (°C) between 2003 and 2013 with delimitation of defined hydrographical provinces: Irish Sea (IS), northern Celtic Sea (nCS), southern CS (sCS), Land's End (LE) waters, northern western English Channel (nWEC) and southern WEC (sWEC). The warmest SSTs are characteristic of seasonally stratified areas and the coldest of permanently well-mixed ecosystems.

column is well-mixed and the warmest SST, areas with seasonal stratification. The Ushant front (Pingree et al., 1975; Morin, 1984, Sournia et al., 1990) separates the seasonally stratified southern Celtic Sea (sCS) and nWEC from the permanently well-mixed sWEC. Such a frontal structure is also observed off the Penwith Peninsula (west of Cornwall, UK), around the Land's End (LE) waters; hereafter we refer to these well-mixed waters as LE. St. George's Channel front separates permanently well-mixed southern IS (sIS) waters from the seasonally stratified northern CS (nCS) waters. In addition to the similar hydrographical properties, the WEC, CS and IS also exhibited similar seasonal dynamics and biogeochemical processes (Pingree et al., 1978; Pemberton et al., 2004; Smyth et al., 2009). Based on these observations, we defined six key hydrographical provinces (Fig. 2) with fixed boundaries, which represent the shifting area of thermal fronts. The use of fixed boundaries allows a direct comparison between the representative provinces.

We did not include coastal areas strongly influenced by riverine inputs (Fig. 2) such as the Bristol Channel, coastal Irish waters, surface waters in vicinity of Plymouth and the eastern part of the sIS (which is also seasonally stratified). We chose to study only the southern part of the IS because of the complexity of the northern IS, which has successive stratified, frontal and mixed systems (Simpson and Hunter, 1974) and is influenced by freshwater inputs (Gowen and Stewart, 1995). The study of the permanently well-mixed part of the IS allowed us to apply our algorithm developed for the sWEC to estimate for the first time air–sea CO$_2$ fluxes

in the IS. In the southwest corner of our study area, at the shelf break, internal tides and turbulence favor vertical mixing which sustains biological activity by supplying nutrients to the photic zone (Pingree et al., 1981; Joint et al., 2001; Sharples and Tweddle, 2007). Because the internal tides at the shelf break induce specific biogeochemical properties and our algorithms are not intended to predict surface pCO$_2$ in this province, we excluded the shelf break region (Fig. 1, southwestern area) from our study area.

3 Material and methods

3.1 FerryBox data sets

From January 2011 to January 2014, a FerryBox system was installed on the Voluntary Observing Ship (VOS) *Armorique* (Brittany Ferries). This vessel crossed the English Channel between Roscoff (France, 48°43′38 N, 3°59′03 E) and Plymouth (United Kingdom, 50°22′12 N, 4°08′31 E; Fig. 1) up to three times a day. The FerryBox continuously measured sea surface temperature (SST), salinity and partial pressure of CO$_2$ (pCO$_2$, from April 2012) along the ferry track with more than 600 crossings with pCO$_2$ acquisition. Between January 2011 and January 2014, discrete sampling was performed on 57 return crossings between Roscoff and Plymouth with a total of 1026 sampling locations in the WEC. During each cruise, 18 water samples were taken from the FerryBox seawater circuit for the determination of dissolved inorganic carbon (DIC), total alkalinity (TA) and associated

salinity and nutrient concentrations (Marrec et al, 2013). Seawater pCO_2 values were calculated from TA, DIC, temperature, salinity and nutrient concentrations with the CO2SYS program (Pierrot et al., 2006) using the equilibrium constants of CO_2 proposed by Mehrbach et al. (1973), refitted by Dickson and Millero (1987) on the seawater pH scale, as recommended by Dickson et al. (2007). The methods used for the analytical determinations of DIC and TA are described in detail in Marrec et al. (2014) and gave accuracies of ± 2 and $3\,\mu mol\,kg^{-1}$, respectively. Thus, the computed values of pCO_2 from DIC and TA have uncertainties at the lower end of $\pm 6\,\mu atm$ (Zeebe and Wolf-Galdrow, 2001). Sensors were calibrated and/or adjusted based on these bimonthly discrete measurements as described in Marrec et al. (2014). Based on the comparison between high-frequency pCO_2 data obtained with a Contros HydroC/CO_2 FT sensor and bimonthly pCO_2 data calculated from DIC/TA, we estimated high-frequency pCO_2 measurements uncertainties at the lower end $\pm 6\,\mu atm$ (Marrec et al., 2014), in the same range as computed values of pCO_2 from DIC and TA. We built a composite monthly data set of in situ SST and pCO_2 data over 3 years based on both high-frequency and bimonthly (twice a month) measurements. We used bimonthly discrete pCO_2 data between January 2011 and April 2012 and high-frequency pCO_2 data from April 2012 to January 2014. The monthly pCO_2 data were then adjusted to reference month July 2012, for MLR computation, using an atmospheric growth rate of $0.15\,\mu atm\,month^{-1}$ ($1.8\,\mu atm\,yr^{-1}$) and assuming that the surface ocean pCO_2 is growing at the same rate as the atmosphere. This growth rate was calculated from atmospheric pCO_2 at Mace Head (Ireland, see Sect. 3.5 for further details) from January 2003 to December 2013 and is then representative of our study area.

3.2 Satellite and other environmental data

Satellite-derived Chl a concentrations ($\mu g\,L^{-1}$) were acquired from the Moderate Resolution Imaging Spectroradiometer (MODIS) aboard the Aqua satellite. Daily images were provided by the Natural Environment Research Council (NERC) Earth Observation Data Acquisition and Analysis Service (NEODAAS) at a spatial resolution of 1.1 km. Monthly mean Chl a estimates were computed from January 2003 to December 2013 from these individual images over our study area (Fig. 1). WEC, CS and IS waters are optically complex shelf waters (Joint and Groom, 2000; Darecki et al., 2003; McKee et al., 2007). These shelf seas present both Case 1 and Case 2 optical water types (Morel and Prieur, 1977; Morel et al., 2006) depending on their hydrographical properties (seasonally stratified or homogeneous), the proximity to the coast, and the period of the year. In Case 1 waters, the optical properties are dominated by chlorophyll and associated degradation products as in open ocean waters. In coastal waters, classified as Case 2, suspended particulate sediments and yellow substances of terrestrial origin induce

important biases on chlorophyll a concentration estimates and special algorithms have been developed for these waters (Gohin et al., 2002). As shown by Groom et al. (2009), who explain how a coastal station in the nWEC (L4) can be considered as Case 1 or Case 2 depending on various parameters, it is difficult to label our studied provinces as Case 1 or Case 2 waters. However sWEC, LE and IS present more similarities with Case 2 waters, especially during winter, whereas nWEC and CS are closer to Case 1 waters. The NEODAAS provided satellite Chl a estimates based on the OC3 algorithm, more specific to Case 1 waters, and on the OC5 algorithm (Gohin et al., 2002), developed in coastal waters of the eastern English Channel and the Bay of Biscay affected riverine input (Seine, Loire, Gironde). Chl a estimates based on the OC3 algorithm show enhanced Chl a concentrations during winter, particularly in near-coast and in well-mixed provinces, whereas Chl a estimates from the OC5 algorithm tend to underestimate the Chl a concentrations especially during spring and summer (data not shown). We chose to use the OC3 algorithm in this study, which seemed more suitable and more representative of the biological activity dynamics, and we gridded monthly 1.1 km satellite data into $0.05° \times 0.05°$ grid cells over our study area. We extracted monthly mean Chl a values along the ship track from January 2011 to December 2013 (Fig. 3b) to predict pCO_2 based on MLRs (see below).

Satellite-based SST (°C) data were acquired from the Advanced Very High Resolution Radiometer (AVHRR) instrument. Monthly mean SST estimates were computed from January 2003 to January 2014 from individual images with a spatial resolution of 1.1 km by the NEODAAS. A validation between monthly in situ SST and associated satellite SST showed a robust correlation ($R^2 = 0.97$, $N = 448$, $p < 0.001$ and RMSE $= 0.43\,°C$). We gridded 1.1 km resolution satellite SST into $0.05° \times 0.05°$ cells as with all other remotely sensed and modeled parameters.

Photosynthetically active radiation (PAR, in $E\,m^{-2}\,d^{-1}$) data were retrieved from the Ocean Biology Processing Group (McClain, 2009; http://oceancolor.gsfc.nasa.gov). We used the Level 3 monthly merged PAR product from MODIS Aqua. PAR was used as a variable in the MLRs as an indicator of the amount of light available for phytoplankton, which presented inter-annual variation over our study period (Fig. 3c). Based on the observations of L'Helguen et al. (1996), Marrec et al. (2014) suggested that light availability might be an important factor responsible for the strong inter-annual variability of phytoplankton blooms in the sWEC.

Mixed layer depth (MLD), which was one of the variables used in algorithm development for the seasonally stratified nWEC and in the spatial extrapolation of this algorithm in the adjacent CS, was computed from the MARS3D model (Lazure and Dumas, 2008; Berger et al., 2014) developed in the PREVIMER project (Charria and Repecaud, 2014). MLD was defined as the shallowest depth corresponding to a tem-
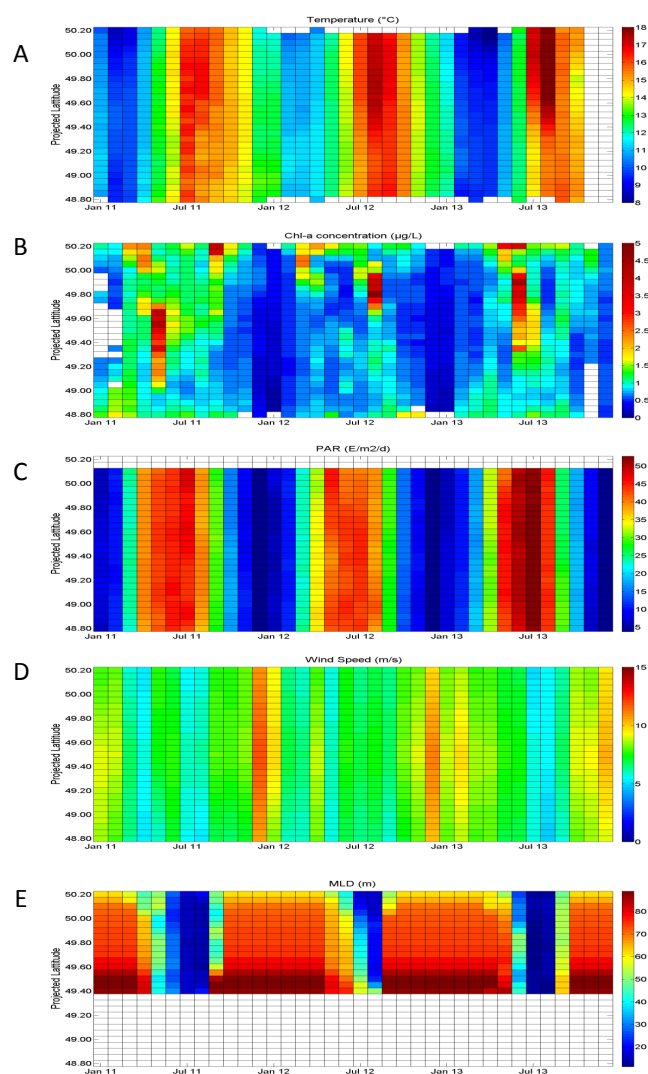
Figure 3. Distribution of monthly gridded **(a)** SST (°C), **(b)** Chl *a* (µg L^{-1}), **(c)** PAR (E m^{-2} d^{-1}), **(d)** wind speed (m s^{-1}) and **(e)** MLD over depth ratio MLDr in the WEC between Roscoff and Plymouth from January 2011 to December 2013.

perature or density difference with the surface water higher than $\delta T = 0.5\,°C$ or $\delta\text{Dens} = 0.125$ (Monterey and Levitus, 1997). We compared the model outputs with MLD calculated from the temperature and salinity profile at the fixed station E1 off Plymouth (50.03° N, 4.37° W; depth 75 m) from January 2006 to January 2014 (Fig. S1 in the Supplement). Measurements were undertaken every 2 weeks by the Western Channel Observatory (NERC National Capability of the Plymouth Marine Laboratory and Marine Biological Association, www.westernchannelobservatory.org.uk). Profiles were obtained by a Seabird SBE 19+ with precision for temperature and computed salinity of 0.005 °C and 0.002, respectively. We also compared the modeled MLD in the CS and at the E1 fixed station with Armor-3D L4 Analysis observation products provided by the Copernicus Ma-

rine Environment Monitoring Service (ex-MyOcean, http://marine.copernicus.eu). The latter are combined products from satellite observations (sea level anomalies, mean dynamic topography and sea surface temperature) and in situ (temperature and salinity profiles) data on a 1/2° regular grid in our study area. Modeled and in situ (from the Western Channel Observatory) MLD at the E1 station showed a robust correlation ($R^2 = 0.82$, $N = 89$, Fig. S1). Comparing modeled and Armor-3D L4 Analysis observation products MLD of CS (Fig. S1) clearly showed the robust approximation of MLD by the model, particularly concerning the start and the end of stratification, despite a small overestimation of the modeled MLD. These comparisons validated the use of modeled MLD in our computations. Modeled MLDs were gridded in the $0.05° \times 0.05°$ grid in seasonally stratified provinces and were extracted along the ship track in the nWEC to be included in the $p\text{CO}_2$ algorithms. We chose to use the MLD over depth ratio (MLDr) in the MLR computation instead of MLD. During winter in seasonally stratified areas, the whole water column is mixed. However, depths are not homogeneous (ranging from -20 to -200 m); thus the use of MLD winter values, which corresponded approximately to the bathymetry, would lead to bias in MLR computation. MLD, in our algorithms, was only an indicator of the presence or absence of stratification of the water column, particularly concerning the start and the end of stratification. Figure 3e shows the monthly MLDr ratio in the nWEC between Roscoff and Plymouth.

Monthly wind speed data (WND, in m s^{-1}) corrected to 10 m height were obtained from four-times-daily wind speed products from the ERA-interim re-analysis project (Dee et al., 2011) produced by the European Centre for Medium-Range Weather Forecasts (ECMWF). We extracted the 0.125° latitude by 0.125° longitude global grid wind speed values over the study area, and we gridded these data into our $0.05° \times 0.05°$ grid. We used WND data in the computation of the gas transfer velocity of CO$_2$ (k) as an indicator of wind stress for the calculation of air–sea CO$_2$ fluxes (Sect. 3.5). Figure 3d shows the monthly WND values used in the algorithm development along the ferry route from 2011 to 2013.

3.3 Development of $p\text{CO}_2$ algorithms

We developed two specific algorithms to estimate surface seawater $p\text{CO}_2$ in each of the hydrographical provinces of the WEC (seasonally stratified nWEC and permanently well-mixed sWEC) in order to apply them on a larger spatial and temporal scale in the adjacent Celtic and Irish seas. We used MLRs to predict $p\text{CO}_2$ in each province based on monthly mean values of Chl *a*, SST, PAR, WND (for the sWEC), MLD (for the nWEC) and from a time variable TI (Eqs. 1 and 2) representative of the seasonality (Friedrich and Oschlies, 2009; Lefèvre et al., 2005; Signorini et al., 2013) ac-

cording to

$$pCO_{2,\mathrm{MLR}} = a_0 + \sum_{i=1}^{n} a_i \cdot p_i \qquad (1)$$

$$\mathrm{TI} = \sin\left(\frac{2 \cdot \pi \cdot (\mathrm{Day} - \alpha)}{365}\right), \qquad (2)$$

where $pCO_{2,\mathrm{MLR}}$ is the predicted pCO_2, a_0 is the intercept of the MLR and a_i is the coefficient related to each variable p_i. In Eq. (2), "Day" is the 15th day of each month (Julian day) and α a value between 0 and 365 chosen by iteration to optimize the seasonal phasing until the minimum standard deviation on residuals and the best correlation coefficient R^2 are obtained by the MLR. All of these parameters were gridded in 0.05° latitude intervals (Fig. 3 and 5) between 48.80° N (off Roscoff) and 50.20° N (off Plymouth). The northern latitude limit of 50.20° N is relatively far from Plymouth in order to exclude effects of freshwater inputs from the Tamar and Plym rivers, which influence the biogeochemical properties of the area (Smyth et al., 2009) and are not representative of nWEC waters. The WEC is divided into sWEC and nWEC at 49.40° N from the average position of the thermal front separating the two hydrographical provinces during the period of study (Fig. 2 and Marrec et al. 2014). MLRs were applied on these gridded monthly values in each province using the "regress" Matlab® function. The performance of regional algorithms was evaluated by the correlation coefficient R^2, the adjusted R^2, the root-mean-square error (RMSE) and the p values (for each of the parameters and for the regression). These parameters represent the capacity (the R^2 and the adjusted R^2) and uncertainty (RMSE) of the algorithms to predict pCO_2. The coefficient of determination R^2 indicates the amount of total variability explained by the regression mode. The adjusted R^2 is the coefficient of determination of the MLR adjusted to the degree of freedom, which depends on the number of variables used. In each MLR presented in the study, the adjusted R^2 and R^2 were similar; thus only R^2 is presented.

MLR coefficients were calculated based on our 3-year data set, and the goal of the study is to apply the algorithms over a decade (2003–2013) over the study area (Fig. 1). Based on the atmospheric pCO_2 calculated from Mace Head atmospheric xCO_2, we calculated a regional anthropogenic increase in atmospheric CO_2 of 1.8 µatm yr^{-1}, a similar rate as mentioned by Thomas et al. (2008) and Le Quéré et al. (2010). We assumed that the ocean surface pCO_2 increase is trending at the same pace as the atmospheric pCO_2. Thus we consider a regional increase of seawater pCO_2 of 1.8 µatm yr^{-1} representative of our study region. When we computed the algorithms, we considered this factor in the computations by adding a correction term ΔX (Eq. 3) on the right term of Eq. (1) (Shadwick et al., 2010; Signorini et al., 2013) with

$$\Delta X = \frac{1.8}{12} \cdot \Delta m, \qquad (3)$$

where Δm (month) is equal to the number of months since July 2012, the middle of our study period (2011–2013). For example, in January 2013, ΔX would be equal to (1.8/12) × (+6) and in January 2012 ΔX would be (1.8/12) × (−6). The same reference month (i.e., July 2012) was used to extrapolate the algorithms from January 2003.

We normalized each of the variables p_i (Eq. 4) using the mean ($p_{i,m}$) and standard deviation ($p_{i,\mathrm{SD}}$) of p_i over the study period. The normalized coefficients, which are directly comparable and dimensionless, allowed us to evaluate the relative contribution, or weight, of each of the independent variables (i.e., SST, Chl a, TI, wind speed, PAR and MLD) in the prediction of the dependent variable (i.e., $pCO_{2,\mathrm{MLR}}$).

$$p_{i,s} = \frac{(p_i - p_{i,m})}{p_{i,\mathrm{SD}}} \qquad (4)$$

3.4 SOCAT and LDEO data

The Surface Ocean CO$_2$ ATlas (SOCAT) database (http://www.socat.info/; Bakker et al., 2014) is an international collection of underway ocean CO$_2$ measurements. This compilation currently includes approximately 10.1 million measurements from more than 2660 data sets from 1968 to 2011. The Lamont–Doherty Earth Observatory (LDEO) pCO_2 database Version 2013 (Takahashi et al., 2014) lists $\sim$ 9 million surface ocean pCO_2 measurements made since 1957. From January 2003 to January 2011, 64 800 pCO_2 and associated SST/SSS values were available over the study area (Fig. 4, Table 1). From 2003 to 2014, in sWEC, nWEC and sCS, pCO_2 values from SOCAT were available for 50 to 65 % of the months (Table 1), mainly from the same southwest–northeast route (Fig. 4) operated principally by three voluntary observing ships (Lüger et al., 2004; Steinhoff, 2010; Schuster et al., 2013; Lefèvre et al., 2014; more details available on the SOCAT website) which crossed these provinces up to twice per month, almost every month from 2003 to 2011. In nCS and IS, the data coverage was sparser and in LE very few data were available. We binned all of these data into the study grid on a monthly basis. We binned the SOCAT and LDEO data into 0.05° × 0.05° grid and computed the mean monthly value in each grid cell. The performance of the model was obtained by comparing the mean observed and predicted monthly value per grid cell (see Fig. S2 and 2). For each province, the observed and predicted monthly mean based on this 0.05° × 0.05° grid in each province are plotted in Fig. 8.

3.5 Calculation of air–sea CO$_2$ fluxes

The fluxes of CO$_2$ across the air–sea interface (F) were computed from the pCO_2 air–sea gradient ($\Delta pCO_2 = pCO_{2\ \mathrm{water}} - pCO_{2\ \mathrm{air}}$, µatm) according to

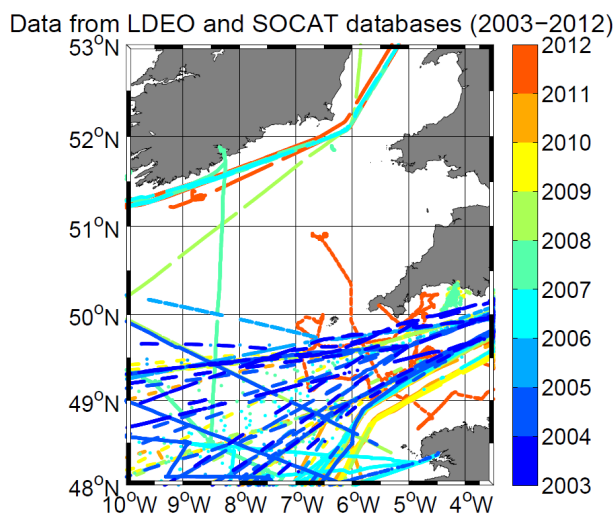$$F = k \cdot K_0 \cdot \Delta pCO_2, \qquad (5)$$

Figure 4. Map of available SOCAT and LDEO surface pCO_2 data with color-coded respective year of acquisition between 2003 and 2011.

Table 1. Area (in km^2) of each defined province (Fig. 2), number of available SOCAT/LDEO pCO_2 data and the percentage of available monthly SOCAT/LDEO pCO_2 data between 2003 and 2011.

Region	Area (km^2)	No. of Obs.	% Time coverage
IS	18 115	2717	10 %
nCS	58 035	5140	11 %
sCS	65 943	40 790	65 %
nWEC	11 912	12 036	62 %
sWEC	12 167	4031	50 %
LE	5412	86	5 %

where k is the gas transfer velocity ($m\,s^{-1}$) and K_0 is the solubility coefficient of CO_2 ($mol\,atm^{-1}\,m^{-3}$) calculated after Weiss (1970). The exchange coefficient k (Eq. 6) was computed as a function of wind speed with the algorithm given by Nightingale et al. (2000) established in the southern bight of the North Sea (SBNS). The SBNS and the WEC present similar environmental characteristics: these two shallow continental shelves are both close to land with high tidal currents controlling the physical structure of the water column.

$$k = \left(0.222 \cdot C_2 \cdot u_{10}^2 + 0.333 \cdot u_{10}\right) \cdot \left(\frac{Sc}{660}\right)^{-0.5}, \quad (6)$$

where u_{10} is the wind speed data at 10 m height ($m\,s^{-1}$), Sc the Schmidt number at in situ SST and C_2 the nonlinearity coefficients for quadratic terms of the gas transfer relationships according to Wanninkhof et al. (2002):

$$C_2 = \left(\frac{1}{n}\sum_{j=1}^{n} u_j^2\right)/u_{mean}^2, \quad (7)$$

where u_j is the high-frequency wind speed ($m\,s^{-1}$), u_{mean} is the monthly mean wind speed ($m\,s^{-1}$) and n the number of available wind speed data in the month. The empirical relationships of gas transfer with wind speed are nonlinear; then, by using monthly mean wind speeds, the temporal distribution of the wind speeds over the month will affect the gas transfer velocity. We apply the same method reported by Jiang et al. (2008) to account for the intrinsic variability of monthly wind speed data.

We also computed gas transfer velocity with the Wanninkhof (1992) and with the Wanninkhof and McGillis (1999) parameterizations for long-term winds to give a range of computed air–sea CO_2 fluxes and we used the nonlinearity coefficients for quadratic and cubic terms of the gas transfer relationship (Wanninkhof et al., 2002; Jiang et al., 2008). Wind speeds along the ferry track and over the study area were extracted from four-times-daily wind speed data corrected at 10 m height from the ERA-interim re-analysis project (Sect. 3.2). Atmospheric pCO_2 ($pCO_{2\,air}$) was calculated from the CO_2 molar fraction (xCO_2) at the Mace Head site (53°33′ N, 9°00′ W; southern Ireland) of the RAMCES network (Observatory Network for Greenhouse gases) and from the water vapor pressure (pH_2O) using the Weiss and Price (1980) equation. Atmospheric pressure (P_{atm}) over the study area was obtained from the ERA-interim re-analysis project (Dee et al., 2011).

To estimate the uncertainties of the monthly air–sea CO_2 flux values, we follow the error propagation method exposed in Omar et al. (2007) and used in Lauvset et al. (2013). Uncertainties were expressed by the random error associated with the monthly flux values (σ_F) according to

$$\sigma_F = \left[\left(\frac{\partial F}{\partial K_0} \times \sigma_{K_0}\right)^2 + \left(\frac{\partial F}{\partial k} \times \sigma_k\right)^2\right]. \quad (8)$$

$$+ \left(\frac{\partial F}{\partial \Delta pCO_2} \times \sigma_{\Delta pCO_2}\right)^2$$

$$+ 2\frac{\partial F}{\partial K_0}\frac{\partial F}{\partial k}\mathrm{Cov}_{K_0 k} + 2\frac{\partial F}{\partial K_0}\frac{\partial F}{\partial \Delta pCO_2}\mathrm{Cov}_{K_0 \Delta pCO_2} \quad (9)$$

$$+ 2\frac{\partial F}{\partial k}\frac{\partial F}{\partial \Delta pCO_2}\mathrm{Cov}_{k \Delta pCO_2}\Bigg]^{1/2},$$

where σ_{K0}, σ_k and $\sigma_{\Delta pCO_2}$ are the uncertainties associated with K_0, k and ΔpCO_2, and Cov_{xy} denotes the covariance between any two parameters x and y. The total uncertainty in k is based on an assumed $1\,m\,s^{-1}$ uncertainty in the wind speed data and from the 0.43 °C uncertainty of the AVHRR satellite-based SST (Sect. 3.2), which impact the Schmidt number calculation and ranged between ± 13 and $\pm 41\,m\,month^{-1}$. The uncertainty in K_0 is obtained by summing a 0.5 % uncertainty in the computation of K_0 (McGillis and Wanninkhof, 2006) and the 0.43 °C error in the AVHRR satellite-based SST, which corresponds to a 1.4 % uncertainty. The uncertainty in K_0 ranged between ± 0.66 and $\pm 0.94\,mol\,C\,m^{-3}\,atm^{-1}$. The total uncertainty in
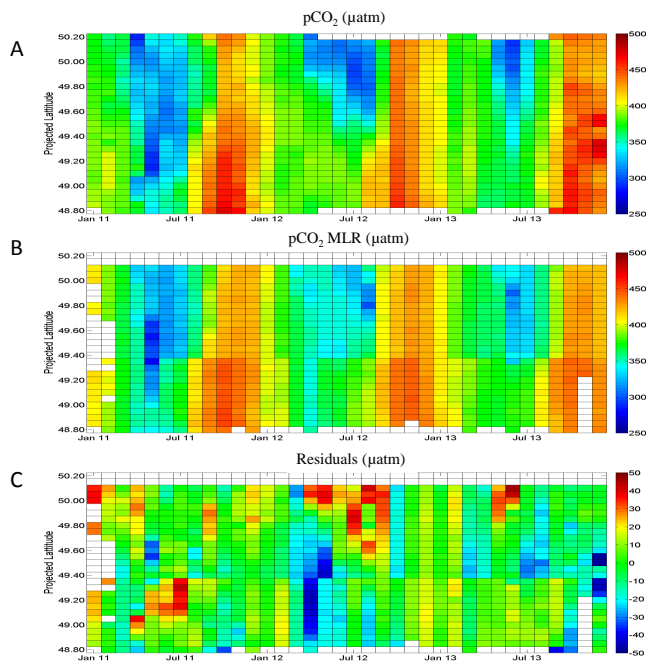
Figure 5. Distribution of monthly gridded **(a)** pCO$_2$ (µatm) based on bimonthly DIC/TA measurements (January 2011 to March 2012) and on high-frequency pCO$_2$ measurements (April 2012 to December 2013) in WEC, **(b)** pCO$_{2,MLR}$ (µatm) computed from nWEC and sWEC algorithms and **(c)** residuals (pCO$_2$−pCO$_{2,\ \text{MLR}}$ in µatm) between Roscoff and Plymouth from January 2011 to December 2013.

ΔpCO$_2$ results from the quadratic sum of the total uncertainty in pCO$_{2,\ \text{MLR}}$ (15.9 µatm in permanently well-mixed provinces and 17.1 µatm in seasonally stratified provinces; Sect. 4.1) and an assumed ±1 µatm uncertainty in the atmospheric pCO$_2$. The covariances were obtained by holding all parameters at their mean values, except SST, and by using the changes in K_0, k and ΔpCO$_2$ due to SST to determine these covariances. Depending on the provinces, Cov$_{K0k}$ varied between −12.96 and −27.61, Cov$_{K0\Delta p\text{CO}_2}$ between 3.15×10^{-5} and 1.05×10^{-4} and Cov$_{k\Delta p\text{CO}_2}$ between -3.94×10^{-4} and -1.05×10^{-4}. For further details on the calculation of the terms used in Eq. (7) see Omar et al. (2007). The random error associated with the mean annual flux estimates was calculated as the quadric sum of the uncertainties in the monthly mean fluxes. Thus, air–sea CO$_2$ fluxes in the paper and figures are given with their computed uncertainties.

4   Results and discussion

4.1   Performance of MLR

We performed MLRs to estimate surface pCO$_2$ based on SST, Chl a, the time variable TI, WND and PAR in the sWEC, and by including MLDr (MLD/depth ratio) and without WND in the nWEC. Table 2 shows the MLR-normalized coefficients used in the algorithms and their evolutions when we added new variables in the computations. The corresponding R^2 and RMSE are the indicators of the performance of the MLR at each addition of a new variable. Based on SST, Chl a, PAR, 398 and 510 monthly gridded observations, we obtained R^2 of 0.61 and 0.69 with RM-SEs of 22.2 and 22.6 µatm, in the sWEC and nWEC respectively (Table 2). The inclusion of WND in sWEC and MLDr in nWEC increased R^2 values up to 0.62 and 0.73 with respective RMSE of 22.2 and 21.0 µatm. The inclusion of the time variable TI considerably improved the performance of the MLR, with R^2 values of 0.80 and 0.82 and RMSEs of 15.9 and 17.1 µatm, in sWEC and nWEC, respectively (Table 2, Fig. 6a and b). It is worth noting that when excluding Chl a in the MLR, R^2 decreased by 0.03 and 0.05 and RMSE increased by 1.4 and 2.1 µatm in sWEC and nWEC, respectively. Overall, the RMSE accounted for less than 10 % of the amplitude of the pCO$_2$ signal (approximately 200 µatm). For each variable and each MLR, we calculated the p values, which were all smaller than 0.001 (not shown in Table 2), meaning that all of the variables were statistically significant in the MLR.

From the normalized coefficients, we calculated the percentages of variability explained by each variable. The seasonal pCO$_2$ signal followed an average dynamic close to a sinusoidal signal, with maximal values in fall and minimal values in spring, with transitional values in winter and summer. Therefore, the time variable TI, which is a sinusoidal function, contributed to more than half of the variability of the pCO$_2$ signal, highlighting the strong seasonality observed on this signal (Fig. 5a, Table 2). Beside TI, the most significant variables in terms of relative contribution were SST and PAR, with 22 and 15 % in sWEC and both with 15 % in nWEC, respectively. Chl a contributed 7 and 6 % in the sWEC and nWEC, respectively, a relatively low value considering that, as reported by Marrec et al. (2013), biological processes are the main driver of seasonal pCO$_2$ variability in the WEC. The addition of MLDr improved the performance of the MLR despite its relatively small contribution compared to the other normalized coefficients. Due to the complexity of the algorithms, a quantitative interpretation of non-normalized coefficients is difficult. For example, according to our model, pCO$_2$ decreases by 14.4 µatm when SST increases by 1 °C (Table 2). This value contradicts the expected thermodynamic relationship between SST and pCO$_2$ from Takahashi et al. (1993). The goal of this study was to develop suitable algorithms to predict pCO$_2$ variability in

Table 2. MLR-normalized coefficients for each variable in sWEC and nWEC with corresponding R^2 and RMSE values. Percentages of variability explained by each variable were computed only when all the variables were included in the MLR. Non-normalized coefficient values are given for the last step of the MLR with their standard error (SE). N values are the number of values used in the MLR and α is the value between 0 and 365 chosen by iteration to optimize the seasonal phasing.

sWEC	48.80–49.40° N							
Variables	MLR coefficient	1	2	3	4	% of variability	Coefficient values	SE
	a0	396.12	397.44	397.45	397.90	–	669.19	19.81
SST	a1	11.43	18.14	17.91	−29.48	22.4 %	−14.39	1.27
Chl a	a2	−16.63	−4.60	−4.80	−8.71	6.6 %	−23.45	2.65
PAR	a3	–	−23.81	−24.79	−20.48	15.5 %	−1.30	0.08
WND	a4	–	–	1.56	−5.84	4.4 %	−4.04	0.83
TI	a5	–	–	–	–67.31	51.1 %	−67.31	3.48
	R^2	0.32	0.61	0.62	0.80		$N = 398$	
	RMSE (µatm)	29.5	22.2	22.2	15.9		$\alpha = 335$	$p < 0.001$
nWEC	49.40–50.20° N							
Variables	MLR coefficient	1	2	3	4	% of variability	Coefficient values	SE
	a0	377.55	377.30	377.14	377.34	–	423.95	12.73
SST	a1	1.59	10.66	17.75	−18.13	14.0 %	−7.34	0.99
Chl a	a2	−22.16	−7.15	−5.22	−8.59	6.7 %	−13.16	1.41
PAR	a3	–	−31.79	−24.03	23.49	18.2 %	1.49	0.20
MLD	a4	–	–	−15.49	−9.05	7.0 %	−29.00	4.62
TI	a5	–	–	–	69.92	54.1 %	69.92	4.33
	R^2	0.29	0.69	0.73	0.82		$N = 510$	
	RMSE (µatm)	34.2	22.6	21.0	17.1		$\alpha = 211$	$p < 0.001$

continental shelf seas by maximizing the performance of the MLR and not to define empirical relationships between the variables and pCO$_2$.

Figures 5a, b and c show the monthly gridded (0.05° of latitude) pCO$_2$, pCO$_2$ predicted from MLR coefficients (pCO$_{2,\text{MLR}}$) and associated residuals (pCO$_{2,\text{obs}}$ − pCO$_{2,\text{MLR}}$) from January 2011 to January 2014 between Roscoff and Plymouth. In the sWEC, pCO$_2$ values lower than 350 µatm were observed during spring 2011, whereas in the same period in 2012 and 2013, pCO$_2$ remained close to the atmospheric equilibrium, between 350 and 400 µatm. Thus, the dynamics of pCO$_2$ in both provinces presented important inter-annual variability. As the pCO$_2$ simulation by the MLR is mainly driven by a seasonal cycle (TI), which is the same every year, these inter-annual discrepancies can yield bias in the MLR simulation. For the sWEC the MLR model overestimated pCO$_2$ during spring and summer 2011 (residuals up to 30 µatm, Fig. 5b and c) and underestimated pCO$_2$ in spring 2012 (residuals down to −50 µatm, Fig. 5b and c) by simulating an average decrease of pCO$_2$ both years. In Fig. 6c and d, residuals are plotted vs. observed pCO$_2$ in the sWEC and nWEC, and in Fig. 6e and f monthly mean residuals over each province are plotted vs. months from January 2011 to December 2013. In the sWEC, when observed pCO$_2$ (pCO$_{2,\text{Obs}}$) values were below 350 µatm,

as in spring 2011, pCO$_{2,\text{MLR}}$ values were much higher than pCO$_{2,\text{Obs}}$ and residuals were highly negative. In the sWEC, residuals as a function of the observed pCO$_2$ were not homogeneously distributed, especially during year 2011 (Fig. 6), with high negative residuals when pCO$_2$ was below 350 µatm and high positive residuals when pCO$_2$ was over 450 µatm. In the nWEC, the distribution of residuals was more homogeneous (Fig. 6c and d); the less pronounced inter-annual variability was responsible for the better performance of the algorithms (R^2) in this part of the WEC.

Shadwick et al. (2010) and Signorini et al. (2013) undertook similar studies on the Scotian shelf and the northeastern American continental shelf, respectively. They estimated pCO$_2$ as a function of SST, Chl a and k, and from SST, salinity, Chl a and a time variable (TI), respectively, using MLR. Based on 14 monthly mean values from a high-frequency data set at a moored buoy, the algorithm developed by Shadwick et al. (2010) attained a R^2 of 0.81 with an associated standard error of 13 µatm. They extrapolated this algorithm over the entire Scotian shelf region to investigate pCO$_2$ and air–sea CO$_2$ fluxes from remotely sensed data from 1999 to 2008. Signorini et al. (2013) reported R^2 and associated RMSE ranging from 0.42 to 0.87 and from 22.4 to 36.9 µatm, respectively. They divided the northeastern American continental shelf into five distinct regions according to their phys-

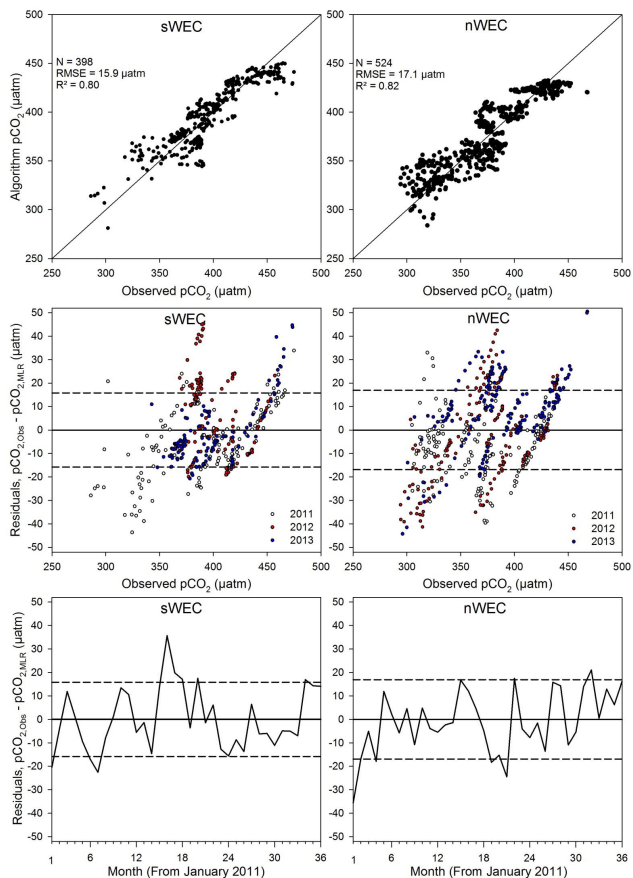**Figure 6.** Observed monthly gridded pCO_2 (µatm) versus $pCO_{2,\,MLR}$ computed from the algorithms developed in sWEC **(a)** and in nWEC **(b)** with respective number of values (N), R^2 and RMSE. Residuals between observed pCO_2 and predicted pCO_2 in function of observed pCO_2 values (µatm) and year of sampling in sWEC **(c)** and nWEC **(d)**. Mean monthly residuals (µatm) over sWEC **(e)** and nWEC **(f)** in function of the months from January 2011. On plots C, D, E and F the dashed lines represent the RMSE of MLR developed in sWEC (±15.9 µatm) and nWEC (±17.1 µatm).

ical and biogeochemical attributes. Their studies were based on SOCAT surface ocean pCO_2, and the environmental variables used to predict pCO_2 came from remotely sensed and modeled data. The performances of our MLRs are within the same range as those in these previous studies. We developed our algorithms based on a 3-year data set obtained during highly contrasting years, which contributed to the robustness of our model to predict a representative seasonal cycle of pCO_2 as seen in the nWEC. However, the WEC is a highly dynamic continental shelf ecosystem characterized by strong inter-annual variations. Very exceptional events, inherent to continental shelf areas, remain difficult to simulate with our method, which explain the lower performances of our MLR for the sWEC, as seen from the high residuals observed during 2012.
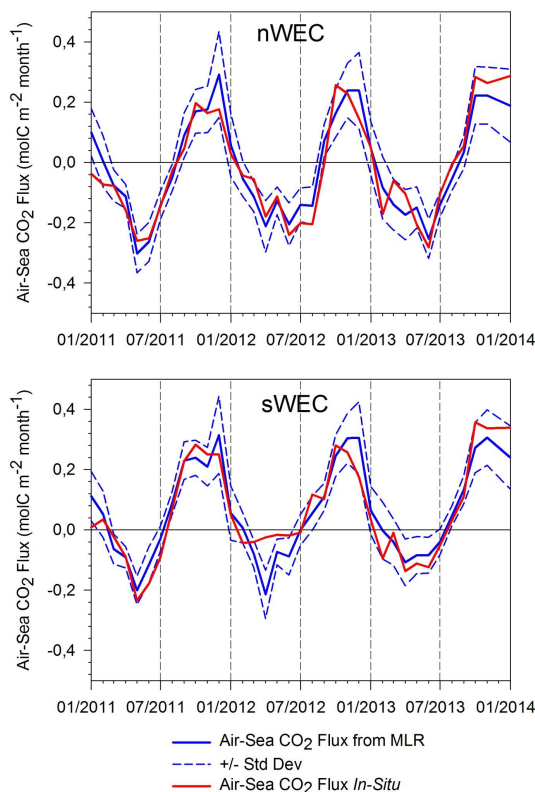

Figure 7. Monthly air–sea CO_2 fluxes (mol C m^{-2} month^{-1}) computed from observed pCO_2 (in red) and $pCO_{2,\,MLR}$ (in blue) data in nWEC and sWEC from 2011 to 2013 using Nightingale et al. (2000) gas transfer velocity K. Dashed lines represent fluxes computed from $pCO_{2,\,MLR}$ plus and minus respective RMSE.

We compared air–sea CO_2 fluxes (Eq. 5) calculated from observed pCO_2 and from pCO_2 simulation (Fig. 7 and Table 3). Figure 7 shows the air–sea CO_2 flux variation in the sWEC and the nWEC based on $pCO_{2,\,obs}$ and $pCO_{2,\,MLR}$ from January 2011 to January 2014. Fluxes were computed from the mean monthly pCO_2 of each province, and the standard deviation on MLR fluxes corresponds to MLR fluxes computed plus and minus the RMSE obtained in the respective provinces (Table 2). Seasonal air–sea CO_2 flux cycles were well described by the algorithm-defined pCO_2, particularly for the nWEC, with both provinces acting as a sink of atmospheric CO_2 during spring and summer and as source of CO_2 to the atmosphere during fall and winter. The inter-annual variability of pCO_2 observed in the sWEC during spring and summer was also reflected in the flux computations, the fluxes based on MLR overestimating the CO_2 sink in spring 2012. Table 3 reports the annual flux estimates in both provinces based on in situ pCO_2 observations and $pCO_{2,\,MLR}$. On an annual scale, the seasonally stratified nWEC waters acted as a sink of atmospheric CO_2 at a rate of 0.0 to 0.5 mol C m^{-2} yr^{-1} based on in situ pCO_2 measurements. Fluxes computed from $pCO_{2,\,MLR}$ also indicated that

Table 3. Air–sea CO$_2$ fluxes (in mol C m^{-2} yr^{-1}) calculated from observed pCO$_2$ and from pCO$_2$ obtained by MLR along the ferry track in nWEC and sWEC using Nightingale et al. (2000) k parameterization. In the main text and figures, all these fluxes are given with their respective uncertainties as computed in Sect. 3.5. Here we provide in brackets values computed using Wanninkhof et al. (1992) and Wanninkhof and McGillis (1999) k parameterizations to give a range of computed air–sea CO$_2$ fluxes.

Year	Northern WEC		Southern WEC	
	Obs.	MLR	Obs.	MLR
2011	−0.5 (−0.9/−0.3)	−0.1 (−0.1/0.2)	0.5 (0.8/0.7)	0.8 (1.3/1.0)
2012	−0.4 (−0.5/−0.2)	−0.2 (−0.4/0.0)	0.8 (1.4/1.1)	0.6 (1.0/0.9)
2013	0.0 (−0.1/0.3)	−0.3 (−0.6/−0.1)	0.7 (1.0/1.0)	0.7 (1.1/1.0)

the nWEC acts as a sink of atmospheric CO$_2$, but we observed some discrepancies between the magnitude of in situ and MLR-based fluxes. The permanently well-mixed sWEC waters acted as a source of CO$_2$ to the atmosphere from 2011 to 2013 ranging between 0.5 and 0.8 mol C m^{-2} yr^{-1}, and annual CO$_2$ fluxes computed from observed and modeled pCO$_2$ were in good agreement. The performances of our algorithms to estimate monthly surface pCO$_2$ allowed us to compute suitable air–sea CO$_2$ fluxes in WEC provinces during three contrasted years.

4.2 Spatial and temporal extrapolation of the algorithms

We applied the previous algorithms (Sect. 4.1) over our study area (Fig. 2) from monthly mean remotely sensed and modeled parameters in the permanently well-mixed sWEC, IS and LE and in the seasonally stratified nWEC, sCS and nCS. The pCO$_2$ values computed from these variables were averaged by province from January 2003 to December 2011 (Fig. 8). The available SOCAT and LDEO observed pCO$_2$ data (Fig. 4 and Table 1) were binned into 0.05° × 0.05° grid cells and averaged over the provinces. Observed pCO$_2$ monthly mean data were superimposed on the algorithm pCO$_2$ time series (Fig. 8).

For the nWEC (Fig. 8d), the modeled data followed the main features of the seasonal cycle described by the observed data and were in relatively good quantitative agreement (see Fig. S2 for more details). Spring pCO$_2$ minima were in the same range, despite the discrepancy of timescales. During fall and winter, maximum values were not always reached, suggesting a relatively small overestimation of modeled pCO$_2$ values at this time. In the sCS (Fig. 8c), where observed data covered most months from 2003 to 2013, predicted data fitted reasonably well the observed pCO$_2$ during spring and summer. During fall and winter, only few observed pCO$_2$ data were above equilibrium values, but the model predicted surface water pCO$_2$ oversaturation compared to atmospheric equilibrium. Despite the limited number of observed data available for the nCS, IS and
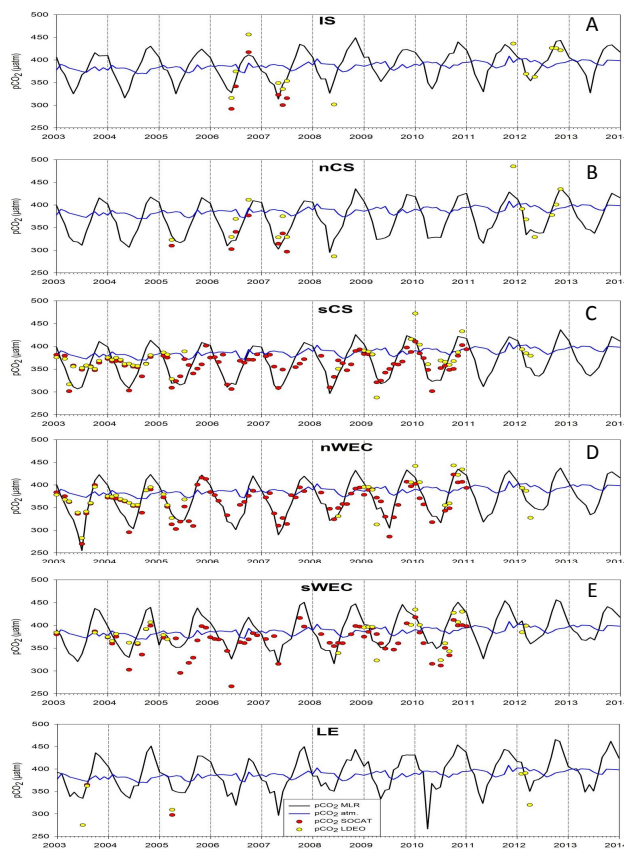

Figure 8. Time series of monthly pCO$_{2, \text{MLR}}$ (µatm, in black) averaged over IS, nCS, sCS, nWEC, sWEC and LE provinces from 2003 to 2013. Monthly mean corresponding to SOCAT data (red dots) and LDEO data (yellow dots) are shown for comparison. The blue lines represent the atmospheric pCO$_2$.

LE, the model predictions were in good agreement with the observed pCO$_2$ (Fig. 8 and S2). For the sWEC (Fig. 8e), the predicted pCO$_2$ values were higher than the observed data, our algorithm thus mainly overestimating the pCO$_2$. During spring, the minimal observed pCO$_2$ values were not always reached by the model. Figure 4 shows that the observed pCO$_2$ data available for the sWEC were acquired along the Ushant front (Pingree et al., 1975; Morin, 1984; Sournia et al., 1990) at the border of the province (sWEC, nWEC and sCS) delimited based on summer SST (Fig. 2). This border is a frontal zone between well-mixed and stratified systems with enhanced biological activity due to the constant supply of nutrients from the deep layer of stratified systems, especially in summer when the winter nutrient stock is totally depleted (Holligan, 1981; Morin, 1984, Le Fèvre, 1986, Le Boyer et al., 2009). This enhanced productivity might induce biological consumption of CO$_2$, which would explain the overestimation of modeled pCO$_2$ in the frontal zone. The SOCAT and LDEO data were not representative of a homogeneous system, hindering a direct comparison.

Directly comparing monthly mean pCO$_2$ values obtained from algorithms and the SOCAT and LDEO pCO$_2$ data could generate an important bias because of the timescale difference between these data sets. Monthly gridded SO-CAT and LDEO data were mainly based on measurements performed at daily scales. Computed pCO$_2$ values were representative of the average monthly pCO$_2$ variability, which tends to smooth extreme values obtained at shorter timescales and prevent any observation of short-term processes. Despite this timescale discrepancy the mean differences between observed and predicted pCO$_2$ were -1 ± 27 in the sCS, -3 ± 25 in the nWEC, 3 ± 26 in the nCS, -7 ± 26 in the IS and -3 ± 29 μatm in LE on an annual scale. Considering the uncertainties relative to the MLR of 17 μatm (Sect. 4.1), these results were very promising and allowed us to validate the extrapolation of our method over our study area. The results obtained in the sWEC, with an annual mean difference of -14 ± 26 μatm, were less promising as explained above and in Sect. 4.1. The comparison of SOCAT and LDEO data with the model predictions provided indications on the MLR performance on a wider spatial scale. For the first time, we thus computed the seasonal and long-term dynamics of pCO$_2$ and associated air–sea CO$_2$ fluxes over a decade for this part of the northwestern European continental shelf (Sect. 4.3) despite the relative uncertainties inherent to the method.

4.3 Dynamics of pCO$_2$ and air–sea CO$_2$ fluxes

4.3.1 Seasonal and biogeochemical controls of pCO$_2$ in stratified ecosystems

Figures 9 to 11 show the monthly values of Chl a, computed pCO$_2$ and associated air–sea CO$_2$ fluxes in the stratified and homogeneous regions of our study area defined in Fig. 2. Based on in situ MLD data at fixed station E1 (Western Channel Observatory of Plymouth, Fig. 1), on MLD from Armor-3D L4 Analysis observation products and on modeled MLD (Sect. 3.2, Fig. S1), we generally observed an onset of stratification in the nWEC and CS from April to October. Modeled MLD data indicated that water column stratification generally started one month earlier and ended one month later in the CS than in the nWEC. The formation of shallow surface layers (≈ 30 m in the CS and 15 m in the nWEC) triggers the initiation of spring phytoplankton blooms in the CS and nWEC (Pingree, 1980). The earlier onset of stratification in the CS than in the nWEC, due to less intense tidal streams (Pingree, 1980), is consistent with the preliminary signs of the spring bloom observed firstly in the CS (Fig. 9) and resulted in pCO$_2$ values below 350 μatm first observed in CS in April and one month later in the nWEC (Fig. 9). In the CS, pCO$_2$ values remained below the atmospheric equilibrium until October despite the apparent lack of biological activity in surface waters (Chl a concentrations < 1 μg L^{-1}). Subsurface phytoplankton blooms can occur within the thermocline
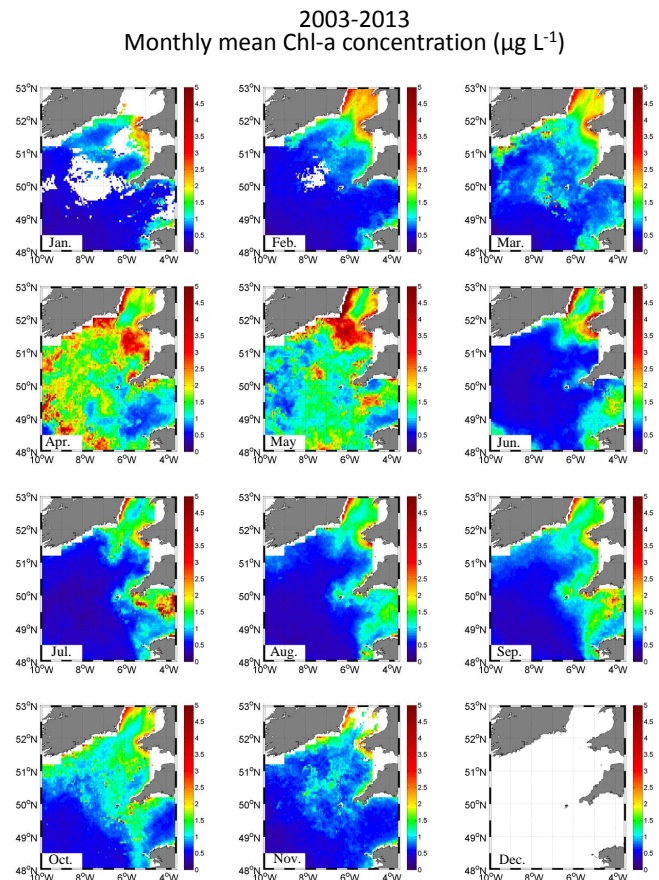

Figure 9. Monthly satellite Chl a (μg L^{-1}) averaged from 2003 to 2013 from January (top left corner) to December (bottom right corner). Satellite Chl a data were not available in December.

at the interface with the deep cold water pool, which is not depleted in nutrients (Pemberton et al., 2004; Southward et al., 2005; Smyth et al., 2009; Hickman et al. 2012), and maintained low pCO$_2$ values. In the nWEC, spring Chl a values remained between 1 and 2 μg L^{-1}, with particularly elevated values in July, resulting in CO$_2$ undersaturated waters with respect to the atmosphere until September. The breakdown of stratification and associated remineralization of organic matter started one month earlier in the nWEC than in the CS and resulted in surface waters oversaturated in CO$_2$ in the two provinces from September and October, respectively. From end of fall to the end of the winter (March of the following year), surface waters remained undersaturated in CO$_2$ with respect to the atmosphere (Fig. 8 and 10) in seasonally stratified systems due to dominant thermodynamical control (Marrec et al., 2013).
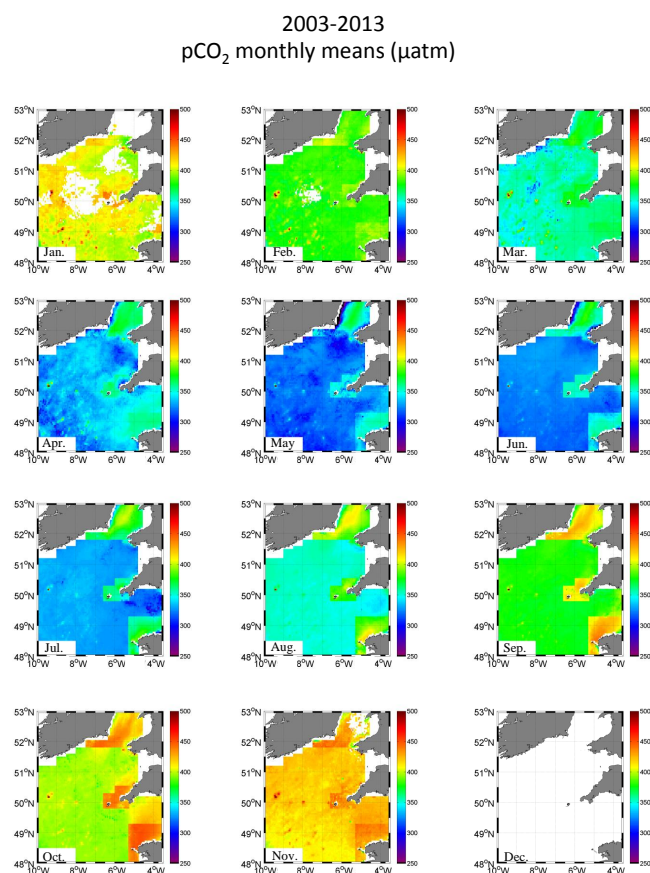
2003-2013
pCO₂ monthly means (µatm)

Figure 10. Monthly $pCO_{2,\,MLR}$ (µatm) computed from the algorithms developed in seasonally stratified and in permanently well-mixed systems, averaged from 2003 to 2013 from January (top left corner) to December (bottom right corner).

4.3.2 Seasonal and biogeochemical controls of pCO_2 in permanently well-mixed ecosystems

The interpretation of the seasonal dynamics of pCO_2 linked to Chl *a* based on satellite observations in the all-year well-mixed sWEC, LE and IS is more complex than in adjacent seasonally stratified systems. In the IS, we obtained abnormally high Chl *a* satellite estimates based on the OC3 algorithm (Sect. 3.2) most of the year caused by elevated suspended particles and colored dissolved organic matter concentrations (McKee and Cunningham, 2006). Moreover, the areas defined as sWEC and LE are not only representative of homogeneous systems, but they also include tidal mixing frontal zones. These frontal regions host higher biological production than well-mixed systems (Pingree et al., 1975), which enhance the Chl *a* signal. The latter had a minor contribution (7 %, Table 2) in the computation of pCO_2 in homogeneous systems and did not have a large effect on pCO_2 prediction. Instead, as reported by previous studies (Boalch et al., 1978; L'Helguen et al., 1996; Wafar et al., 1983), the main factor controlling phytoplankton production in homo-

geneous ecosystems is the light availability, represented in the MLR by the PAR. The PAR contributed to 16 % of the variability of computed pCO_2 and was concomitant with the observed CO₂ undersaturation from April to July. In June, when day length was the longest and meteorological conditions were generally favorable, we observed peaks in Chl *a* values associated with the lowest pCO_2 values (Fig. 8 and 10) of 320 µatm as biology exerted a dominant control on the pCO_2 signal (Marrec et al., 2013). The productive period is shorter in all-year well-mixed systems than in seasonally stratified areas (Marrec et al., 2013, 2014). Surface pCO_2 values were below the atmospheric equilibrium from March to July in the sWEC, LE and IS, whereas these patterns were observed from March to September/October in the CS and the nWEC (Fig. 8 and 10). This is also due to the fact that at the end of summer the organic matter remineralization processes started earlier in homogeneous systems and surface seawaters were oversaturated in CO₂ compared to the atmosphere in August in these ecosystems. The pCO_2 values reached maximum values around 450 µatm during fall in sWEC, LE and IS. Similarly to stratified systems, the well-mixed surface waters remained undersaturated in CO₂ with respect to the atmosphere (Fig. 8 and 10) during the following winter months due to dominant thermodynamical control (Marrec et al., 2013).

The alternate control of the pCO_2 seasonality by biological processes during spring, summer and fall and by thermodynamic in winter–summer transitions is representative of temperate coastal ecosystems in Europe (Borges et al., 2006; Bozec et al., 2005; Bozec et al., 2006). The separation in fixed representative provinces based on physical properties provides insight on the different phases and amplitudes of the pCO_2 seasonality in these poorly explored ecosystems. The sharp boundaries of pCO_2 (Fig. 10) between permanently well-mixed and seasonally stratified systems can appear as surprising, especially between August and October. However, previous studies in the WEC (Marrec et al., 2013, 2014) showed important pCO_2 gradient from 50 µatm to 100 µatm between sWEC and nWEC surface waters. In August and September 2014 we performed crossings from a newly exploited VOS, the *Pont-Aven* (Brittany Ferries), between Roscoff and Cork (Ireland) and had access to pCO_2 data from DIC/TA measurements in the CS (Fig. S3). By comparing these in situ pCO_2 data with mean pCO_2 data along the ferry tracks calculated from our MLR from 2003 to 2013, we clearly observed the presence of these sharp boundaries between sWEC and nWEC provinces and between nWEC, LE and CS waters. We choose to fix the delimitation of these provinces based on the averaged July and August SST from 2003 to 2013 (Sect. 2, Fig. 2). These regional boundaries represent the shifting area of thermal fronts. As we could not estimate pCO_2 using our algorithms in frontal zones, such an approach appeared suitable.

Table 4. Annual air–sea CO_2 fluxes (in mol C m^{-2} yr^{-1}) in the seasonally stratified (nCS, sCS and nWEC) and permanently mixed provinces (sWEC, LE and IS) of our study area between 2003 and 2013 and the mean annual fluxes over the decade using Nightingale et al. (2000) k parameterization. Scaled annual fluxes over province areas (Table 2) in Tg C yr^{-1} were calculated from the mean annual fluxes over the decade. Fluxes in brackets were calculated using Wanninkhof et al. (1992) and Wanninkhof and McGillis (1999) k parameterizations. Values in italic correspond to the minimal and maximal air–sea CO_2 flux values computed in each province.

| Year | Seasonally stratified | | | Permanently mixed | | |
	nCS	sCS	nWEC	sWEC	LE	IS
2003	−0.7 (−1.1/−0.5)	−0.9 (−1.5/−0.8)	−0.6 (−0.9/−0.3)	0.0 (0.0/0.2)	0.2 (0.2/0.4)	0.0 (0.0/0.2)
2004	−0.5 (−0.8/−0.4)	−0.7 (−1.2/−0.7)	−0.3 (−0.5/−0.2)	0.3 (0.4/0.4)	0.7 (1.2/0.9)	0.4 (0.7/0.6)
2005	−0.6 (−0.9/−0.4)	−0.9 (−1.5/−0.7)	−0.4 (−0.7/−0.2)	0.1 (0.1/0.2)	0.4 (0.7/0.6)	0.4 (0.6/0.7)
2006	−0.9 (−1.6/−0.8)	−1.2 (−2.0/−1.2)	−0.9 (−1.5/−0.8)	−0.1 (−0.3/−0.1)	0.0 (0.0/0.1)	−0.1 (−0.3/0.0)
2007	*−1.0 (−1.7/−1.0)*	*−1.3 (−2.3/−1.5)*	*−1.2 (−2.1/−1.3)*	*−0.7 (−1.4/−1.1)*	*−0.6 (−1.3/−0.9)*	*−0.3 (−0.8/−0.4)*
2008	−0.5 (−0.8/−0.4)	−0.7 (−1.3/−0.7)	−0.4 (−0.8/−0.3)	0.1 (0.0/0.2)	0.3 (0.5/0.5)	0.5 (0.6/0.6)
2009	*−0.4 (−0.6/0.1)*	*−0.4 (−0.6/0.1)*	*0.0 (0.2/0.6)*	*0.8 (1.4/1.3)*	0.7 (1.4/1.3)	*0.7 (1.3/1.0)*
2010	−0.5 (−0.7/−0.3)	−0.7 (−1.1/−0.5)	−0.2 (−0.2/0.1)	0.6 (1.1/0.8)	0.6 (1.0/0.9)	0.6 (1.0/0.8)
2011	−0.7 (−1.2/−0.6)	−0.9 (−1.5/−0.8)	−0.5 (−0.9/−0.4)	0.3 (0.5/0.4)	0.4 (0.6/0.5)	0.3 (0.4/0.4)
2012	−0.7 (−1.2/−0.6)	−0.7 (−1.3/−0.7)	−0.4 (−0.7/−0.3)	0.4 (0.6/0.6)	*0.8 (1.3/1.0)*	0.5 (0.9/0.7)
2013	−0.8 (−1.4/−0.8)	−1.1 (−2.0/−1.2)	−0.5 (−1.1/−0.4)	0.1 (−0.1/0.2)	0.4 (0.6/0.6)	0.3 (0.3/0.4)
Mean (mol C m^{-2} yr^{-1})	−0.6 (−1.1/−0.5)	−0.9 (−1.5/−0.8)	−0.5 (−0.8/−0.3)	0.2 (0.2/0.3)	0.3 (0.6/0.5)	0.3 (0.4/0.5)
Mean (Tg C yr^{-1})	−0.45 (−0.77/−0.36)	−0.69 (−1.16/−0.63)	−0.07 (−0.12/−0.05)	0.02 (0.03/0.04)	0.02 (0.04/0.04)	0.06 (0.09/0.10)

4.3.3 Variability of air–sea CO_2 fluxes over the shelf and the decade

On an annual scale, the permanently well-mixed sWEC, IS and LE acted as net sources of CO_2 to the atmosphere at a mean rate (from 2003 to 2013) of 0.2 ± 0.2, 0.3 ± 0.2 and 0.3 ± 0.3 mol C m^{-2} yr^{-1}, respectively, (Table 4) whereas the seasonally stratified systems acted as net sinks of atmospheric CO_2, with mean values over 11 years of -0.6 ± 0.3, -0.9 ± 0.3 and -0.5 ± 0.3 mol C m^{-2} yr^{-1} for the nCS, sCS and nWEC, respectively (Table 4). Air–sea CO_2 fluxes computed from predicted pCO_2 corroborate the hypothesis of Borges et al. (2005), with permanently well-mixed systems acting as sources of CO_2 to the atmosphere and seasonally stratified systems acting as a sink of atmospheric CO_2. The only previous flux estimate for the CS was based on a study by Frankignoulle and Borges (2001), reported in Borges et al. (2006), which indicated that the CS acts as sink of CO_2 of -0.8 mol C m^{-2} yr^{-1}. In the sCS we obtained an averaged flux value of -0.9 ± 0.3 mol C m^{-2} yr^{-1}, which is in agreement with this previous study. Further, we report what is, to the best of our knowledge, the first estimate of air–sea CO_2 flux in the IS of 0.3 ± 0.2 mol C m^{-2} yr^{-1}. These values are all on the same order as the mean annual air–sea CO_2 flux value of -1.9 mol C m^{-2} yr^{-1} for European coastal waters reported by Borges et al. (2006). The good agreement between the compilations of annually integrated fluxes computed from field measurements by Borges et al. (2006) and the results found in this study further support the robustness of our MLR.

Our study provides a first assessment of the seasonality of pCO_2 and air–sea CO_2 fluxes over 11 years as well as of the inter-annual and multi-annual variability. Monthly surface ocean pCO_2 derived from algorithms (Fig. 8) showed important inter-annual variability for the seasonal cycle of CO_2 in each province. Monthly air–sea CO_2 fluxes (Fig. 12) followed the same trend as pCO_2, resulting in significant inter-annual differences in the intensity and/or direction of annual fluxes (Table 4 and Fig. 12). The IS and LE remained over-all annual sources of CO_2 to the atmosphere from 2003 to 2013, except in 2007 when they acted as sinks of atmospheric CO_2. In the sWEC, the annual 11-year average flux value of 0.2 ± 0.2 mol C m^{-2} yr^{-1} corresponds to annual values ranging from -0.7 ± 0.2 to 0.8 ± 0.3 mol C m^{-2} yr^{-1}. The sWEC acted as a sink of atmospheric CO_2 in 2006 and 2007, and as a source of CO_2 to the atmosphere or neutral for the other years. In 2007, in permanently well-mixed systems, a particularly intense spring phytoplankton bloom (data not shown) occurred, which resulted in important CO_2 undersaturation and a CO_2 sink. The CO_2 outgassing during fall 2007 was one of the lowest observed over the decade (Fig. 12), due to relatively weak wind speeds at this time (data not shown) and resulting low k values. The association of these two features explained the annual CO_2 sink obtained in 2007. Seasonally stratified systems showed variability in the intensity of annual air–sea CO_2 fluxes but remained sinks of atmospheric pCO_2 over the decade, except the nWEC in 2009. In addition to the changes of ocean–atmosphere pCO_2 gradient, the wind-dependent gas transfer velocity has a strong influence on air–sea CO_2 fluxes. For example, during fall 2009, monthly pCO_2 values were in the same range as the other years (Fig. 8) but we observed peaks of CO_2 outgassing in response to more intense monthly wind speeds (> 10 m s^{-1}). As mentioned above in Sect. 4.1, our method precluded establishment of empirical relationships between the variables and pCO_2, and it is therefore difficult to quantitatively and
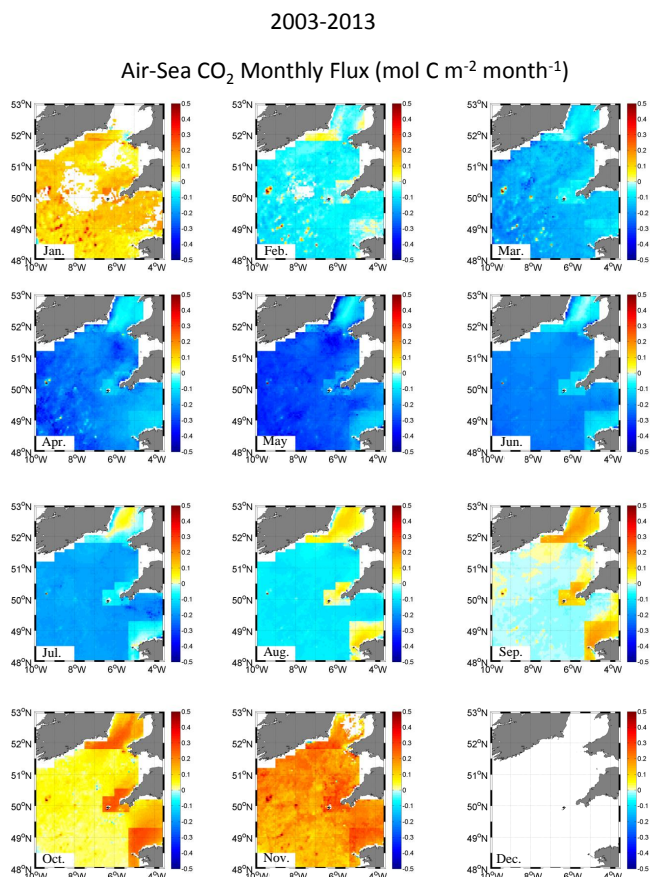
2003-2013

Air-Sea CO$_2$ Monthly Flux (mol C m^{-2} month^{-1})

Figure 11. Monthly air–sea CO$_2$ fluxes (mol C m^{-2} month^{-1}) computed from pCO$_{2,\,\mathrm{MLR}}$ and using Nightingale et al. (2000) K–wind relationship, averaged from 2003 to 2013 from January (top left corner) to December (bottom right corner). Negative values indicate CO$_2$ sink.

Figure 12. Monthly air–sea CO$_2$ fluxes (black lines, left-hand side y axis, mol C m^{-2} month^{-1}) computed from pCO$_{2,\,\mathrm{MLR}}$ and using Nightingale et al. (2000) K–wind relationship in IS (**a**), nCS (**b**), sCS (**c**), nWEC (**d**), sWEC (**e**) and LE (**f**) provinces from 2003 to 2013. Negative values indicate CO$_2$ sink. Integrated annual CO$_2$ fluxes (vertical grey bars, right-hand side y axis, mol C m^{-2} yr^{-1}). The dashed line corresponds to the monthly fluxes plus and minus the calculated uncertainties, and the error bars correspond to the annual computed uncertainties (details in Sect. 3.5).

directly interpret the influence of each variable in the pCO$_2$ simulation.

We scaled the mean annual fluxes over province areas (Tables 1 and 4) and obtained air–sea CO$_2$ fluxes of -0.45 ± 0.21, -0.69 ± 0.23 and -0.07 ± 0.04 Tg C yr^{-1} in the nCS, sCS and nWEC, and of 0.02 ± 0.03, 0.02 ± 0.02 and 0.06 ± 0.04 Tg C yr^{-1} in the sWEC, LE and IS, respectively. These fluxes correspond to absorption of -1.11 ± 0.32 Tg C yr^{-1} over our study area (the total uncertainty was calculated as the quadratic sum of uncertainties in each province). Borges et al. (2006) estimated the CO$_2$ sink over the European continental shelves at -68.1 Tg C yr^{-1}, while Chen and Borges (2009) reported air–sea CO$_2$ flux of -16.1 Tg C yr^{-1} in the northeastern Atlantic continental shelf region. The contribution of our study area, which represents 5 % of the European continental shelf reported by Borges et al. (2006), appears rather small because of the large extent of well-mixed ecosystems. However, considering the lack of investigation of air–sea CO$_2$ fluxes in the CS, IS and to a lesser extent in the WEC, our study allowed for the first
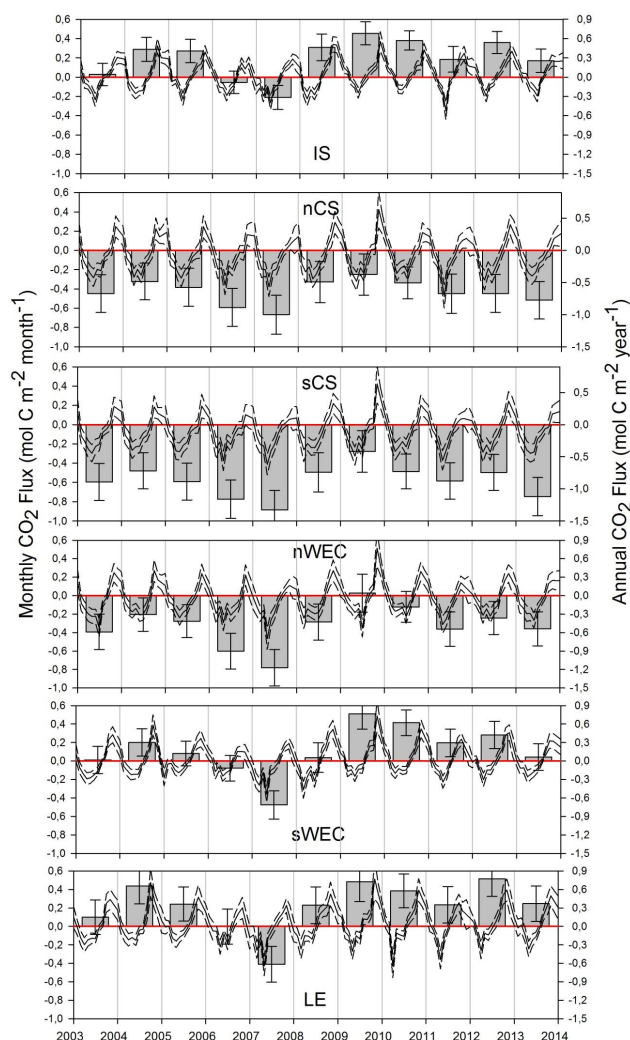
time the estimation of the spatiotemporal dynamics of air–sea CO$_2$ fluxes in these provinces of the northwestern European shelf.

5 Concluding remarks and perspectives

Based on a 3-year data set of pCO$_2$ measurements acquired on a VOS in the WEC, we estimated surface ocean pCO$_2$ and air–sea CO$_2$ fluxes in the northwestern European continental shelf waters using MLRs from remotely sensed SST, Chl a, PAR and wind speed (in the sWEC), from modeled

MLD (in the nWEC) and from a time variable TI. For the first time, seasonal and long-term dynamics of pCO$_2$ and air–sea CO$_2$ fluxes over this part of the northwestern European continental shelf were evaluated over a decade, despite the relatively high uncertainties inherent to such method. We thus provide the first estimate of air–sea CO$_2$ flux in the poorly documented CS, IS and WEC. As mentioned above, very few data are currently available in these coastal seas. However, the number of surface in situ pCO$_2$ data grows exponentially and these data are now easily available on data portals such as SOCAT and LDEO to develop and validate such algorithms. For example, in situ data of the CO$_2$ system are currently acquired during seasonal cruises within the CANDYFLOSS project (NERC, collaboration National Oceanographic Center/Biological Station of Roscoff) in the CS and the IS, and with a FerryBox system operating between Roscoff (France) and Cork (Ireland). In the future, these data will improve and allow further developments of our algorithms with an adequate division of the shelf area in representative biogeochemical provinces and by developing specific algorithms in each province.

The reconstructed decadal data sets highlighted the importance of multi-annual study of air–sea CO$_2$ fluxes in continental shelf seas. As mentioned by Keller et al. (2014), it can be difficult to detect relevant trends in the seawater pCO$_2$ signal, particularly in coastal areas with high inter- and intra-annual variability. Beaugrand et al. (2000) and Tréguer et al. (2014) demonstrated that coastal marine systems of western Europe are connected to large-scale North Atlantic atmospheric circulation, the North Atlantic Oscillation (NAO), and there is a consensus that these coastal systems are highly sensitive to natural and anthropogenic climate change (Goberville et al., 2010, 2014). Thomas et al. (2008) investigated the influence of the NAO on air–sea CO$_2$ fluxes in the North Atlantic and suggested that multi-annual variability of the ocean CO$_2$ system was linked to the NAO phasing. Salt et al. (2013) demonstrated the connection between NAO forcings and pH and CO$_2$ variability in the North Sea, another shelf sea of the northwestern European continental shelf. We did not attempt an evaluation of the long-term trend of our CO$_2$ signal as we believe our algorithm needs to be further improved with more in situ data as mentioned above. In the future, a similar approach could be applied on our data set to investigate the possible links between large-scale climatic indices and the multi-annual variability of pCO$_2$ and air–sea CO$_2$ on this part of the northwestern European continental shelf, which is closely connected to North Atlantic open ocean waters.

The Supplement related to this article is available online at doi:10.5194/bg-12-5371-2015-supplement.

References

Bakker, D. C. E., Pfeil, B., Smith, K., Hankin, S., Olsen, A., Alin, S. R., Cosca, C., Harasawa, S., Kozyr, A., Nojiri, Y., O'Brien, K. M., Schuster, U., Telszewski, M., Tilbrook, B., Wada, C., Akl, J., Barbero, L., Bates, N. R., Boutin, J., Bozec, Y., Cai, W.-J., Castle, R. D., Chavez, F. P., Chen, L., Chierici, M., Currie, K., de Baar, H. J. W., Evans, W., Feely, R. A., Fransson, A., Gao, Z., Hales, B., Hardman-Mountford, N. J., Hoppema, M., Huang, W.-J., Hunt, C. W., Huss, B., Ichikawa, T., Johannessen, T., Jones, E. M., Jones, S. D., Jutterström, S., Kitidis, V., Körtzinger, A., Landschützer, P., Lauvset, S. K., Lefèvre, N., Manke, A. B., Mathis, J. T., Merlivat, L., Metzl, N., Murata, A., Newberger, T., Omar, A. M., Ono, T., Park, G.-H., Paterson, K., Pierrot, D., Ríos, A. F., Sabine, C. L., Saito, S., Salisbury, J., Sarma, V. V. S. S., Schlitzer, R., Sieger, R., Skjelvan, I., Steinhoff, T., Sullivan, K. F., Sun, H., Sutton, A. J., Suzuki, T., Sweeney, C., Takahashi, T., Tjiputra, J., Tsurushima, N., van Heuven, S. M. A. C., Vandemark, D., Vlahos, P., Wallace, D. W. R., Wanninkhof, R., and Watson, A. J.: An update to the Surface Ocean CO$_2$ Atlas (SOCAT version 2), Earth Syst. Sci. Data, 6, 69–90, doi:10.5194/essd-6-69-2014, 2014.

Bauer, J. E., Cai, W.-J., Raymond, P. A., Bianchi, T. S., Hopkinson, C. S., and Regnier, P. A. G.: The changing carbon cycle of the coastal ocean, Nature, 504, 61–70, doi:10.1038/nature12857, 2013.

Beaugrand, G., Ibanez, F., and Reid, P. C.: Spatial, seasonal and long-term fluctuations of plankton in relation to hydroclimatic features in the English Channel, Celtic Sea and Bay of Biscay, Mar. Ecol.-Prog. Ser., 200, 93–102, 2000.

Berger, B. H., Dumas, F., Petton, S., and Lazure, P.: Evaluation of the hydrology and dynamics of the operational Mars3d configuration of the bay of Biscay, Mercator Ocean-Quaterly Newsletter, 49, 60–68, 2014.

Boalch, G. T., Harbour, D. S., and Butler, A. I.: Seasonal phytoplankton production in the western English Channel 1964–1974, J. Mar. Biol. Assoc. UK., 58, 943–953, 1978.

Borges, A. V. and Frankignoulle, M.: Distribution of surface carbon dioxide and air-sea exchange in the English Channel and adjacent areas, J. Geophys. Res., 108, 1–14, doi:10.1029/2000JC000571, 2003.

Borges, A. V. and Gypens, N.: Carbonate chemistry in the coastal zone responds more strongly to eutrophication than to ocean acidification, Limnol. Oceanogr., 55, 1–8, 2010.

Borges, A. V., Delille, B., and Frankignoulle, M.: Budgeting sinks and sources of CO$_2$ in the coastal ocean: Diversity of ecosystems counts, Geophys. Res. Lett., 32, L14601, doi:10.1029/2005GL023053, 2005.

Borges, A. V., Schiettecatte, L.-S., Abril, G., Delille, B., and Gazeau, F.: Carbon dioxide in European coastal waters, Estuar. Coast. Shelf S., 70, 375–387. doi:10.1016/j.ecss.2006.05.046, 2006.

Borges, A. V., Alin, S. R., Chavez, F. P., Vlahos, P., Johnson, K. S., Holt, J. T., Balch, W. M., Bates, N., Brainard, R., Cai, W. J., Chen, C. T. A., Currie, K., Dai, M., Degrandpre, M., Delille, B., Dickson, A., Evans, W., Feely, R. A., Friederich, G. E., Gong, G.-C., Hales, B., Hardman-Mountford, N., Hendee, J., Hernandez-Ayon, J. M., Hood, M., Huertas, E., Hydes, D., Ianson, D., Krasakopoulou, E., Litt, E., Luchetta, A., Mathis, J., McGillis, W. R., Murata, A., Newton, J., Ólafsson, J., Omar, A., Perez, F. F., Sabine, C., Salisbury, J. E., Salm, R., Sarma, V. V. S. S., Schneider, B., Sigler, M., Thomas, H., Turk, D., Vandemark, D., Wanninkhof, R., and Ward, B.: A global sea surface carbon observing system: inorganic and organic carbon dynamics in coastal oceans, Proceedings of OceanObs'09: Sustained Ocean Observations and Information for Society (Vol. 2), Venice, Italy, 21–25 September 2009, edited by: Hall, J., Harrison, D. E., and Stammer, D., ESA Publication WPP-306, 2010a.

Borges, A. V., Ruddick, K., Lacroix, G., Nechad, B., Asteroca, R., Rousseau, V., and Harlay, J.: Estimating pCO$_2$ from remote sensing in the Belgian coastal zone, ESA Special Publications, 686, 2–7, 2010b.

Bozec, Y., Thomas, H., Elkalay, K., and de Baar, H. J. W.: The continental shelf pump for CO$_2$ in the North Sea – evidence from summer observation, Mar. Chem., 93, 131–147, doi:10.1016/j.marchem.2004.07.006, 2005.

Bozec, Y., Thomas, H., and Schiettecatte, L.-S.: Assessment of the processes controlling seasonal variations of dissolved inorganic carbon in the North Sea, Limnol. Oceanogr., 51, 2746–2762, 2006.

Cai, W.-J.: Estuarine and coastal ocean carbon paradox: CO$_2$ sinks or sites of terrestrial carbon incineration?, Annu. Rev. Mar. Sci., 3, 123–145, doi:10.1146/annurev-marine-120709-142723, 2011.

Cai, W.-J., Dai, M., and Wang, Y.: Air-sea exchange of carbon dioxide in ocean margins: A province-based synthesis, Geophys. Res. Lett., 33, 1–4, doi:10.1029/2006GL026219, 2006.

Charria, G. and Repecaud, M.: PREVIMER: A contribution to in situ coastal observing systems, Mercator Ocean – Quaterly Newsletter, 49, 9–20, 2014.

Chen, C. A. and Borges, A. V.: Reconciling opposing views on carbon cycling in the coastal ocean?: Continental shelves as sinks and near-shore ecosystems as sources of atmospheric CO$_2$, Deep-Sea Res. Pt. II, 56, 578–590, doi:10.1016/j.dsr2.2008.12.009, 2009.

Chierici, M., Olsen, A., Johannessen, T., Trinañes, J., and Wanninkhof, R.: Algorithms to estimate the carbon dioxide uptake in the northern North Atlantic using shipboard observations, satellite and ocean analysis data, Deep-Sea Res. Pt. II, 56, 630–639, doi:10.1016/j.dsr2.2008.12.014, 2009.

Chierici, M., Signorini, S. R., Mattsdotter-Björk, M., Fransson, A., and Olsen, A.: Surface water fCO$_2$ algorithms for the high-latitude Pacific sector of the Southern Ocean, Remote Sens. Environ., 119, 184–196, doi:10.1016/j.rse.2011.12.020, 2012.

Darecki, M., Weeks, A., Sagan, S., Kowalczuk, P., and Kaczmarek, S.: Optical characteristics of two contrasting Case 2 waters and their influence on remote sensing algorithms, Cont. Shelf Res., 23, 237–250, doi:10.1016/S0278-4343(02)00222-4, 2003.

Dee, D. P., Uppala, S. M., Simmons, A. J., Berrisford, P., Poli, P., Kobayashi, S., Andrae, U., Balmaseda, M. A., Balsamo, G., Bauer, P., Bechtold, P., Beljaars, A. C. M., van de Berg, L., Bidlot, J., Bormann, N., Delsol, C., Dragani, R., Fuentes, M., Geer, A. J., Haimberger, L., Healy, S. B., Hersbach, H., Hólm, E. V., Isaksen, L., Kållberg, P., Köhler, M., Matricardi, M., McNally, A. P., Monge-Sanz, B. M., Morcrette, J.-J., Park, B.-K., Peubey, C., de Rosnay, P., Tavolato, C., Thépaut, J.-N., and Vitart, F.: The ERA-Interim reanalysis: configuration and performance of the data assimilation system, Q. J. R. Meteorol. Soc., 137, 553–597, doi:10.1002/qj.828, 2011.

Dickson, A. G. and Millero, F. J.: A comparison of the equilibrium constants for the dissociation of carbonic acid in seawater media, Deep-Sea Res., 34, 1733–1743, 1987.

Dickson, A. G., Sabine, C. L., and Christian, J. R.: Guide to best practices for ocean CO$_2$ measurements, PICES Special Publication 3, IOCCP report No. 8, 191 pp., 2007.

Dumousseaud, C., Achterberg, E. P., Tyrrell, T., Charalampopoulou, A., Schuster, U., Hartman, M., and Hydes, D. J.: Contrasting effects of temperature and winter mixing on the seasonal and inter-annual variability of the carbonate system in the Northeast Atlantic Ocean, Biogeosciences, 7, 1481–1492, doi:10.5194/bg-7-1481-2010, 2010.

Frankignoulle, M., Borges, A. V.: European continental shelf as a significant sink for atmospheric carbon dioxide, Global Biogeochem. Cy., 15, 569–576, doi:10.1029/2000GB001307, 2001.

Friedrich, T. and Oschlies, A.: Neural network-based estimates of North Atlantic surface pCO$_2$ from satellite data: A methodological study, J. Geophys. Res., 114, 1–12, doi:10.1029/2007JC004646, 2009.

Gattuso, J. P., Frankignoulle, M., and Wollast, R.: Carbon and carbonate metabolism in coastal aquatic ecosystems, Annu. Rev. Ecol. Sys., 29, 405–434, 1998.

Gledhill, D. K., Wanninkhof, R., Millero, F. J., and Eakin, M.: Ocean acidification of the Greater Caribbean Region 1996–2006, J. Geophys. Res., 113, 1–11, doi:10.1029/2007JC004629, 2008.

Goberville, E., Beaugrand, G., Sautour, B., Tréguer, P., and Somlit, T.: Climate-driven changes in coastal marine systems of western Europe, Mar. Ecol.-Prog. Ser., 408, 129–147, doi:10.3354/meps08564, 2010.

Goberville, E., Beaugrand, G., and Edwards, M.: Synchronous response of marine plankton ecosystems to climate in the Northeast Atlantic and the North Sea, J. Marine Syst., 129, 189–202, doi:10.1016/j.jmarsys.2013.05.008, 2014.

Gohin, F., Druon, J. N., and Lampert, L.: A five channel chlorophyll concentration algorithm applied to SeaWiFS data processed by SeaDAS in coastal waters, Int. J. Remote Sens., 23, 1639–1661, 2002.

Gowen, R. J. and Stewart, B. M.: Regional differences in stratification and its effect on phytoplankton production and biomass in the northwestern Irish Sea, J. Plankton Res., 17, 753–769, 1995.

Groom, S., Martinez-Vicente, V., Fishwick, J., Tilstone, G., Moore, G., Smyth, T., and Harbour, D.: The Western English Channel observatory: Optical characteristics of station L4, J. Marine Syst., 77, 278–295, doi:10.1016/j.jmarsys.2007.12.015, 2009.

Hales, B., Strutton, P.G., Saraceno, M., Letelier, R., Takahashi, T., Feely, R., Sabine, C., and Chavez, F.: Satellite-based prediction of pCO$_2$ in coastal waters of the eastern North Pacific, Prog. Oceanogr., 103, 1–15, doi:10.1016/j.pocean.2012.03.001, 2012.

Hickman, A., Moore, C., Sharples, J., Lucas, M., Tilstone, G., Krivtsov, V., and Holligan, P.: Primary production and nitrate uptake within the seasonal thermocline of a stratified shelf sea, Mar. Ecol.-Prog. Ser., 463, 39–57, doi:10.3354/meps09836, 2012.

Hill, E., Brown, J., Fernand, L., Holt, J., Horsburgh, K. J., Proctor, R., Raine, R., and Turrell, W. R.: Thermohaline circulation of shallow tidal seas, Geophys. Res. Lett., 35, L11605, doi:10.1029/2008GL033459, 2008.

Holligan, P. M.: Biological implications of fronts on the northwest European continental shelf, Philos. T. R. Soc. S-A, 302, 547–562, 1981.

IPCC: Climate Change 2013: The Physical Science Basis. Contribution of Working Group I to the Fifth Assessment Report of the Intergovernmental Panel on Climate Change edited by: Stocker, T. F., Qin, D., Plattner, G.-K., Tignor, M., Allen, S.K., Boschung, J., Nauels, A., Xia, Y., Bex, V., and Midgley, P. M., Cambridge University Press, Cambridge, United Kingdom and New York, NY, USA, 1535 pp., 2013.

Jiang, L.-Q., Cai, W.-J., Wanninkhof, R., Wang, Y., and Lüger H.: Air-sea CO_2 fluxes on the U.S. South Atlantic Bight: Spatial and seasonal variability, J. Geophys. Res., 113, C07019, doi:10.1029/2007JC004366, 2008.

Jo, Y.-H., Dai, M., Zhai, W., Yan, X.-H., and Shang, S.: On the variations of sea surface pCO$_2$ in the northern South China Sea: A remote sensing based neural network approach, J. Geophys. Res., 117, 1–13, doi:10.1029/2011JC007745, 2012.

Joint, I. and Groom, S.: Estimation of phytoplankton production from space: current status and future potential of satellite remote sensing, J. Exp. Mar. Biol. Ecol., 250, 233–255, 2000.

Joint, I., Wollast, R., Chou, L., Batten, S., Elskens, M., Edwards, E., Hirst, A., Burkill, P., Groom, S., Gibb, S., Miller, A., Hydes, D., Dehairs, F., Antia, A., Barlow, R., Rees, A., Pomroy, A., Brockmann, U., Cummings, D., Lampitt, R., Loijens, M., Mantoura, F., Miller, P., Raabe, T., Alvarez-Salgado, X., Stelfox, C., and Woolfenden, J.: Pelagic production at the Celtic Sea shelf break, Deep-Sea Res. Pt. II, 48, 3049–3081, doi:10.1016/S0967-0645(01)00032-7, 2001.

Keller, K. M., Joos, F., and Raible, C. C.: Time of emergence of trends in ocean biogeochemistry, Biogeosciences, 11, 3647–3659, doi:10.5194/bg-11-3647-2014, 2014.

Kitidis, V., Hardman-Mountford, N. J., Litt, E., Brown, I., Cummings, D., Hartman, S., Hydes, D., Fishwick, J. R., Harris, C., Martinez-Vicente, V., Woodward, E. M. S., and Smyth, T. J.: Seasonal dynamics of the carbonate system in the Western English Channel, Cont. Shelf Res., 42, 30–40, doi:10.1016/j.csr.2012.04.012, 2012.

L'Helguen, S., Madec, C., and Le Corre, P.: Nitrogen uptake in permanently well-mixed temperate coastal waters., Estuar. Coast. Shelf S., 42, 803–818, doi:10.1006/ecss.1996.0051, 1996.

Lauvset, S.K., Chierici, M., Counillon, F., Omar, A., Nondal, G., Johannessen, T., and Olsen, A.: Annual and seasonal fCO$_2$ and air–sea CO_2 fluxes in the Barents Sea, J. Marine Sys., 113–114, 62–74, doi:10.1016/j.jmarsys.2012.12.011, 2013.

Lazure, P. and Dumas, F.: An external–internal mode coupling for a 3D hydrodynamical model for applications at regional scale (MARS), Adv. Water Resour., 31, 233–250, doi:10.1016/j.advwatres.2007.06.010, 2008.

Le Boyer, A., Cambon, G., Daniault, N., Herbette, S., Le Cann, B., Marié, L., and Morin, P.: Observations of the Ushant tidal front in September 2007, Cont. Shelf Res., 29, 1026–1037, doi:10.1016/j.csr.2008.12.020, 2009.

Le Quéré, C., Takahashi, T., Buitenhuis, E. T., Rödenbeck, C., and Sutherland, S. C.: Impact of climate change and variability on the global oceanic sink of CO_2, Global Biogeochem. Cy., 24, GB4007, doi:10.1029/2009GB003599, 2010.

Le Fèvre, J.: Aspects of the biology of frontal systems, Adv. Mar. Biol., 23, 163–299, 1986.

Lefèvre, N., Aiken, J., Rutllant, J., Daneri, G., Lavender, S., and Smyth, T.: Observations of pCO$_2$ in the coastal upwelling off Chile: Spatial and temporal extrapolation using satellite data, J. Geophys. Res., 107, 8–1, 2002.

Lefèvre, N., Watson, A. J., and Watson, A. R.: A comparison of multiple regression and neural network techniques for mapping in situ pCO$_2$ data, Tellus B, 57, 375–384, 2005.

Lefèvre, N., Urbano, D.F., Gallois, F., and Diverrès, D.: Impact of physical processes on the seasonal distribution of the fugacity of CO_2 in the western tropical Atlantic, J. Geophys. Res.-Oceans, 119, 646–663, doi:10.1002/2013JC009248, 2014.

Liu, K.-K., Atkinson, L., Quinones, R., and Talaue-McManus, L. (Eds.): Carbon and Nutrient Fluxes in Continental Margins A Global Synthesis, IGBP Book Series, Springer, Heidelberg, Germany, 744 pp., 2010.

Lohrenz, S. E., Cai, W.-J.: Satellite ocean color assessment of air-sea fluxes of CO_2 in a river-dominated coastal margin, Geophys. Res. Lett., 33, 2–5, doi:10.1029/2005GL023942, 2006.

Lüger, H., Wallace, D. W. R., Körtzinger, A., and Nojiri, Y.: The pCO$_2$ variability in the midlatitude North Atlantic Ocean dur-

ing a full annual cycle, Global Biogeochem. Cy., 18, GB3023, doi:10.1029/2003GB002200, 2004.

Marrec, P., Cariou, T., Collin, E., Durand, A., Latimier, M., Macé, E., Morin, P., Raimund, S., Vernet, M., and Bozec, Y.: Seasonal and latitudinal variability of the CO$_2$ system in the western English Channel based on Voluntary Observing Ship (VOS) measurements, Mar. Chem., 155, 29–41, 2013.

Marrec, P., Cariou, T., Latimier, M., Macé, E., Morin, P., Vernet, M., and Bozec, Y.: Spatio-temporal dynamics of biogeochemical processes and air–sea CO$_2$ fluxes in the Western English Channel based on two years of FerryBox deployment, J. Marine Syst., doi:10.1016/j.jmarsys.2014.05.010, 2014.

McClain, C. R.: A decade of satellite ocean color observations, Annu. Rev. Mar. Sci., 1, 19–42, doi:10.1146/annurev.marine.010908.163650, 2009.

McGillis, W. R. and Wanninkhof, R.: Aqueous CO$_2$ gradients for air–sea flux estimates, Mar. Chem. 98, 100–108, 2006.

McKee, D. and Cunningham, A.: Identification and characterisation of two optical water types in the Irish Sea from in situ inherent optical properties and seawater constituents, Estuar. Coast. Shelf S., 68, 305–316, doi:10.1016/j.ecss.2006.02.010, 2006.

McKee, D., Cunningham, A., and Dudek, A.: Optical water type discrimination and tuning remote sensing band-ratio algorithms: Application to retrieval of chlorophyll and Kd(490) in the Irish and Celtic Seas, Estuar. Coast. Shelf S., 73, 827–834, doi:10.1016/j.ecss.2007.03.028, 2007.

Mehrbach, C., Culberso, C., Hawley, J. E., and Pytkowic, R. M.: Measurement of apparent dissociation constants of carbonic acid in seawater at atmospheric pressure, Limnol. Oceanogr., 18, 897–907, 1973.

Monterey, G. and Levitus, S.: Seasonal variability of mixed layer depth for the world ocean, NOAA Atlas, NESDIS 14, Washington D.C., 96 pp., 1997.

Morel, A. and Prieur, L.: Analysis of variations in ocean color, Limnol. Oceanogr., 22, 709–722, doi:10.4319/lo.1977.22.4.0709, 1977.

Morel, A., Gentili, B., Chami, M., and Ras, J.: Bio-optical properties of high chlorophyll Case 1 waters and of yellow-substance-dominated Case 2 waters, Deep-Sea Res. Pt. I, 53, 1439–1459, doi:10.1016/j.dsr.2006.07.007, 2006.

Morin, P.: Evolution des éléments nutritifs dans les systems frontaux de l'Iroise: assimilation et regeneration; relation avec les structures hydrologiques et les cycles de développemnt du phytoplankton, PhD thesis in the Univ. Bretagne Occid., 320 pp., 1984.

Muller-Karger, F. E., Varela, R., Thunell, R., Luerssen, R., Hu, C., and Walsh J. J.: The importance of continental margins in the global carbon cycle, Geophys. Res. Lett., 32, L01602, doi:10.1029/2004GL021346, 2005.

Nightingale, P. D., Malin, G., Law, C. S., Watson, A. J., Liss, P. S., Liddicoat, M. I., and Boutin, J., Upstill-Goddard, R. C.: In situ evaluation of air-sea gas exchange parameterizations using novel conservative and volatile tracers, Global Biogeochem. Cy., 14, 373–387, 2000.

Olsen, A., Triñanes, J., and Wanninkhof, R.: Sea–air flux of CO$_2$ in the Caribbean Sea estimated using in situ and remote sensing data, Remote Sens. Environ., 89, 309–325, doi:10.1016/j.rse.2003.10.011, 2004.

Omar, A. M., Johannessen, T., Olsen, A., Kaltin, S., and Rey, F.: Seasonal and interannual variability of the air–sea CO$_2$ flux in the Atlantic sector of the Barents Sea, Mar. Chem., 104, 203-213, doi:10.1016/j.marchem.2006.11.002, 2007.

Omar, A. M., Olsen, A., and Johannessen, T.: Spatiotemporal variations of fCO$_2$ in the North Sea, Ocean Sci., 6, 77–89, 2010, http://www.ocean-sci.net/6/77/2010/.

Ono, T., Saino, T., Kurita, N., and Sasaki, K.: Basin-scale extrapolation of shipboard pCO$_2$ data by using satellite SST and Chl a, Int. J. Remote Sens., 25, 3803–3815, 2004.

Padin, X. A., Vazquezrodriquez, M., Rios, A. F., and Perez, F. F.: Surface CO$_2$ measurements in the English Channel and Southern Bight of North Sea using voluntary observing ships, J. Marine Syst., 66, 297–308, doi:10.1016/j.jmarsys.2006.05.011, 2007.

Padin, X. A., Navarro, G., Gilcoto, M., Rios, A. F., and Pérez, F. F.: Estimation of air–sea CO$_2$ fluxes in the Bay of Biscay based on empirical relationships and remotely sensed observations, J. Marine Syst., 75, 280–289, doi:10.1016/j.jmarsys.2008.10.008, 2009.

Pemberton, K., Rees, A. P., Miller, P. I., Raine, R., and Joint, I.: The influence of water body characteristics on phytoplankton diversity and production in the Celtic Sea, Cont. Shelf Res., 24, 2011–2028, doi:10.1016/j.csr.2004.07.003, 2004.

Pierrot, D., Lewis, E., and Wallace, D. W. R.: MS Excel Program Developed for CO$_2$ System Calculations, ORNL/CDIAC-105, Carbon Dioxide Information Analysis Center, Oak Ridge National Laboratory, U.S. Department of Energy, Oak Ridge, Tennessee, 2006.

Pingree, R. D. and Griffiths, D. K.: Tidal fronts on the shelf seas around the British Isles, J. Geophys. Res., 83, 4615–4622, 1978.

Pingree, R. D., Pugh, P. R., Holligan, P. M., and Forster, G. R.: Summer phytoplankton blooms and red tides along tidal fronts in the approaches to the English Channel, Nature, 258, 672–677, 1975.

Pingree, R. D., Holligan, P. M., and Mardell, G. T.: The effects of vertical stability on phytoplankton distributions in the summer on the northwest European Shelf, Deep-Sea Res., 25, 1011–1028, 1978.

Pingree, R. D.: Physical oceanography of the Celtic Sea and the English Channel, in: The Northwest European Shelf Seas: The Sea-bed and the Sea in Motion, edited by: Banner, F. T., Collins, B., and Massie, K. S., Elsevier, Amsterdam, 638 pp., 1980.

Pingree, R. D., Mardell G. T., and Cartwright, D. E.: Slope Turbulence, internal waves and phytoplankton growth at the Celtic Seas shelf-break, Philos. T. R. Soc. A, 302, 663–682, 1981.

Prowe, A. E. F., Thomas, H., Pätsch, J., Kühn, W., Bozec, Y., Schiettecatte, L.-S., Borges, A. V., and de Baar, H. J.W.: Mechanisms controlling the air–sea CO$_2$ flux in the North Sea, Cont. Shelf Res., 29, 1801–1808, doi:10.1016/j.csr.2009.06.003, 2009.

Rangama, Y., Boutin, J., Etcheto, J., Merlivat, L., Takahashi, T., Delille, B., Frankignoulle, M., and Bakker D. C. E.: Variability of the net air-sea CO$_2$ flux inferred from shipboard and satellite measurements in the Southern Ocean south of Tasmania and New Zealand, J. Geophys. Res., 110, 1–17, doi:10.1029/2004JC002619, 2005.

Reid, P. C., Auger, C., Chaussepied, M., and Burn, M.: The channel, report on sub-region 9, quality status report of the North Sea 1993 (Eds.), UK Dep. of the Environ., Républ. Fr. Minist. de

l'Environ., Inst. Fr. de Rech. Pour l'Exploit. de la Mer, Brest. 153 pp, 1993.

Salisbury, J., Vandemark, D., Hunt, C., Campbell, J., McGillis, W., Mcdowell, W.: Seasonal observations of surface waters in two Gulf of Maine estuary-plume systems: Relationships between watershed attributes, optical measurements and surface pCO$_2$, Estuar. Coast. Shelf S., 77, 245–252, doi:10.1016/j.ecss.2007.09.033, 2008.

Salt, L. A., Thomas, H., Prowe, A. E. F., Borges, A. V., Bozec, Y., and de Baar, H. J. W.: Variability of North Sea pH and CO$_2$ in response to North Atlantic Oscillation forcing, J. Geophys. Res., 118, 1584–1592, doi:10.1002/2013JG002306, 2013.

Schneider, B., Kaitala, S., Mand aunula, P.: Identification and quantification of plankton bloom events in the Baltic Sea by continuous pCO$_2$ and chlorophyll a measurements on a cargo ship, J. Marine Syst., 59, 238–248, doi:10.1016/j.jmarsys.2005.11.003, 2006.

Schneider, B., Gustafsson, E., and Sadkowiak, B.: Control of the mid-summer net community production and nitrogen fixation in the central Baltic Sea: An approach based on pCO$_2$ measurements on a cargo ship, J. Marine Syst., 136, 1–9, doi:10.1016/j.jmarsys.2014.03.007, 2014.

Schiettecatte, L.-S., Thomas, H., Bozec, Y., and Borges, A.V.: High temporal coverage of carbon dioxide measurements in the Southern Bight of the North Sea, Mar. Chem., 106, 161–173, doi:10.1016/j.marchem.2007.01.001, 2007.

Schuster, U., McKinley, G. A., Bates, N., Chevallier, F., Doney, S. C., Fay, A. R., González-Dávila, M., Gruber, N., Jones, S., Krijnen, J., Landschützer, P., Lefèvre, N., Manizza, M., Mathis, J., Metzl, N., Olsen, A., Rios, A. F., Rödenbeck, C., Santana-Casiano, J. M., Takahashi, T., Wanninkhof, R., and Watson, A. J.: An assessment of the Atlantic and Arctic sea-air CO$_2$ fluxes, 1990–2009, Biogeosciences, 10, 607–627, doi:10.5194/bg-10-607-2013, 2013.

Shadwick, E. H., Thomas, H., Comeau, A., Craig, S. E., Hunt, C. W., and Salisbury, J. E.: Air-Sea CO$_2$ fluxes on the Scotian Shelf: s easonal to multi-annual variability, Biogeosciences, 7, 3851–3867, doi:10.5194/bg-7-3851-2010, 2010.

Sharples, J. and Tweddle, J. F.: Spring-neap modulation of internal tide mixing and vertical nitrate fluxes at a shelf edge in summer, Limnol. Oceanogr., 52, 1735–1747, 2007.

Signorini, S. R., Mannino, A., Najjar, R. G., Friedrichs, M. A. M., Cai, W.-J., Salisbury, J., Wang, Z. A., Thomas, H., and Shadwick, E. H.: Surface ocean pCO$_2$ seasonality and sea-air CO$_2$ flux estimates for the North American east coast, J. Geophys. Res., 118, 5439–5460, doi:10.1002/jgrc.20369, 2013.

Simpson, J. H. and Hunter, J. R.: Fronts in the Irish Sea, Nature, 250, 404–406, 1974.

Simpson, J. H., Crisp, D. J., and Hearn, C.: The shelf-sea fronts: Implications of their existence and behavior, Philos. T. R. Soc. A, 302, 531–546, 1981.

Smyth, T. J., Fishwick, J. R., AL-Moosawi, L., Cummings, D. G., Harris, C., Kitidis, V., Rees, A., Martinez-Vicente, V., and Woodward, E. M. S.: A broad spatio-temporal view of the Western English Channel observatory, J. Plankton Res., 32, 585–601, doi:10.1093/plankt/fbp128, 2009.

Sournia, A., Brylinski, J. M., and Dallot, S.: Fronts hydrologiques au large des côtes françaises: Les sites-ateliers de programme Frontal, Oceanol. Acta, 13, 413–438, 1990.

Southward, A. J., Langmead, O., Hardman-Mountford, N. J., Aiken, J., Boalch, G. T., Dando, P. R., Genner, M. J., Joint, I., Kendall, M. A., Halliday, N. C., Harris, R. P., Leaper, R., Mieszkowska, N., Pingree, R. D., Richardson, A. J., Sims, D. W., Smith, T., Walne, A. W., and Hawkins, S. J.: Long-term oceanographic and ecological research in the Western English Channel, Adv. Mar. Biol., 47, 1–105, 2005.

Steinhoff, T.: Carbon and nutrient fluxes in the North Atlantic Ocean, Dissertation, http://eldiss.uni-kiel.de/macau/receive/dissertation_diss_00005704 (last access: 9 September 2011), 2010.

Takahashi, T., Olafson, J., Goddard, J. G., Chipman, D. W., and Sutherland, S. C.: Seasonal variation of CO$_2$ and nutrients in the high-latitude surface oceans: A comparative study, Global Biogeochem. Cy., 7, 843–878, 1993.

Takahashi, T., Sutherland, S. C., and Kozyr, A.: Global Ocean Surface Water Partial Pressure of CO$_2$ Database: Measurements Performed During 1957-2013 (Version 2013), ORNL/CDIAC-160, NDP-088(V2013), Carbon Dioxide Information Analysis Center, Oak Ridge National Laboratory, U.S. Department of Energy, Oak Ridge, Tennessee, doi:10.3334/CDIAC/OTG.NDP088(V2013), 2014.

Telszewski, M., Chazottes, A., Schuster, U., Watson, A. J., Moulin, C., Bakker, D. C. E., González-Dávila, M., Johannessen, T., Körtzinger, A., Lüger, H., Olsen, A., Omar, A., Padin, X. A., Ríos, A. F., Steinhoff, T., Santana-Casiano, M., Wallace, D. W. R., and Wanninkhof, R.: Estimating the monthly pCO$_2$ distribution in the North Atlantic using a self-organizing neural network, Biogeosciences, 6, 1405–1421, doi:10.5194/bg-6-1405-2009, 2009.

Thomas, H., Bozec, Y., Elkalay, K., and de Baar, H. J. W.: Enhanced open ocean storage of CO$_2$ from shelf sea pumping, Science, 304, 1005–1008, doi:10.1126/science.1095491, 2004.

Thomas, H., Bozec, Y., Elkalay, K., de Baar, H. J. W., Borges, A. V., and Schiettecatte, L.-S.: Controls of the surface water partial pressure of CO$_2$ in the North Sea, Biogeosciences, 2, 323–334, doi:10.5194/bg-2-323-2005, 2005.

Thomas, H., Prowe, F. E., Lima, I. D., Doney, S. C., Wanninkhof, R., Greatbatch, R. J., Schuster, U., and Corbière, A.: Changes in the North Atlantic Oscillation influence CO$_2$ uptake in the North Atlantic over the past 2 decades, Global Biogeochem. Cy., 22, GB4027, doi:10.1029/2007GB003167, 2008.

Tréguer, P., Goberville, E., Barrier, N., L'Helguen, S., Morin, P., Bozec, Y., Rimmelin-Maury, P., Czamanski, M., Grosssteffan, E., Cariou, T., Répécaud, M., and Quéméner, L.: Large and local-scale influences on physical and chemical characteristics of coastal waters of Western Europe during winter, J. Marine Syst., 139, 79–90, doi:10.1016/j.jmarsys.2014.05.019, 2014.

Tsunogai, S., Watanabe, S., and Sato, T.: Is there a "continental shelf pump" for the absorption of atmospheric CO$_2$?, Tellus B, 51, 701–712, 1999.

Wafar, M. V. M., Corre, P. L., and Birrien, J. L.: Nutrients and primary production in permanently well-mixed temperate coastal waters, Estuar. Coast. Shelf S., 17, 431–446, 1983.

Wallace, R. B., Baumann, H., Grear, J. S., Aller, R. C., and Gobler, C. J.: Coastal ocean acidification: The other eutrophication problem, Estuar. Coast. Shelf S., 148, 1–13, doi:10.1016/j.ecss.2014.05.027, 2014.

Walsh, J. J.: Importance of continental margins in the marine bio-geochemical cycling of carbon and nitrogen, Nature, 350, 53–55, 1991.

Walsh, J. J., Rowe, G. T., Iverson, R. L., and McRoy, C. P.: Biological export of shelf carbon is a sink of the global CO$_2$ cycle, Nature, 291, 196–201, 1981.

Wanninkhof, R.: Relationship between wind speed and gas exchange over the ocean, J. Geophys. Res., 97, 7373–7382, doi:10.1029/92JC00188, 1992.

Wanninkhof, R. and McGillis, W. R.: A cubic relationship between air-sea CO$_2$ exchange and wind speed, Geophys. Res. Lett., 26, 1889–1892, 1999.

Wanninkhof, R., Doney, S. C., Takahashi, T., and McGillis, W. R.: The effect of using time-averaged winds on regional air-sea CO$_2$ fluxes, in Gas Transfer at Water Surfaces, Geophys. Monogr. Ser., edited by: Donelan, M. A., Drennan, W. M., Saltzman, E. S. and Wanninkhof, R., vol. 127, 351– 356, AGU, Washington, D. C., 2002.

Weiss, R. F.: Solubility of nitrogen, oxygen and argon in water and seawater, Deep-Sea Res, 17, 721–735, 1970.

Weiss, R. F., and Price, B. A.: Nitrous oxide solubility in water and seawater, Mar. Chem., 8, 347–359, 1980.

Zeebe R. E. and Wolf-Gladrow, D. A.: CO$_2$ in seawater: equilibrium, kinetics, isotopes, Elsevier Oceanography Series, 65, Amsterdam, 346 pp., 2001.